UCLA
UCLA Previously Published Works

Title

The Redistribution of Drosophila Vesicular Monoamine Transporter Mutants from Synaptic Vesicles to Large Dense-Core Vesicles Impairs Amine-Dependent Behaviors

Permalink

https://escholarship.org/uc/item/2cc9b5f4

Journal

Journal of Neuroscience, 34(20)

ISSN

0270-6474

Authors

Grygoruk, Anna

Chen, Audrey

Martin, Ciara A

et al.

Publication Date

2014-05-14

DOI

10.1523/jneurosci.0694-14.2014

Copyright Information

Peer reviewed

Cellular/Molecular

The Redistribution of *Drosophila* Vesicular Monoamine Transporter Mutants from Synaptic Vesicles to Large Dense-Core Vesicles Impairs Amine-Dependent Behaviors

Anna Grygoruk,[1] **Audrey Chen,**[1,2] **Ciara A. Martin,**[1,3] **Hakeem O. Lawal,**[1] **Hao Fei,**[1] **Gabriel Gutierrez,**[1] **Traci Biedermann,**[1] **Rod Najibi,**[1] **Richard Hadi,**[1] **Amit K. Chouhan,**[4] **Niall P. Murphy,**[1] **Felix E. Schweizer,**[2] **Gregory T. Macleod,**[4] **Nigel T. Maidment,**[1] **and David E. Krantz**[1]

[1]Department of Psychiatry and Biobehavioral Sciences, Semel Institute for Neuroscience and Human Behavior, Hatos Center for Neuropharmacology, David Geffen School of Medicine, [2]Department of Neurobiology, and [3]Interdepartmental Program in Molecular Toxicology, University of California, Los Angeles, Los Angeles, California 90095, and [4]Department of Physiology, University of Texas Health Science Center, San Antonio, San Antonio, Texas 78229

Monoamine neurotransmitters are stored in both synaptic vesicles (SVs), which are required for release at the synapse, and large dense-core vesicles (LDCVs), which mediate extrasynaptic release. The contributions of each type of vesicular release to specific behaviors are not known. To address this issue, we generated mutations in the C-terminal trafficking domain of the *Drosophila* vesicular monoamine transporter (DVMAT), which is required for the vesicular storage of monoamines in both SVs and LDCVs. Deletion of the terminal 23 aa (DVMAT-Δ3) reduced the rate of endocytosis and localization of DVMAT to SVs, but supported localization to LDCVs. An alanine substitution mutation in a tyrosine-based motif (DVMAT-Y600A) also reduced sorting to SVs and showed an endocytic deficit specific to aminergic nerve terminals. Redistribution of DVMAT-Y600A from SV to LDCV fractions was also enhanced in aminergic neurons. To determine how these changes might affect behavior, we expressed DVMAT-Δ3 and DVMAT-Y600A in a *dVMAT* null genetic background that lacks endogenous *dVMAT* activity. When expressed ubiquitously, DVMAT-Δ3 showed a specific deficit in female fertility, whereas DVMAT-Y600A rescued behavior similarly to DVMAT-wt. In contrast, when expressed more specifically in octopaminergic neurons, both DVMAT-Δ3 and DVMAT-Y600A failed to rescue female fertility, and DVMAT-Y600A showed deficits in larval locomotion. DVMAT-Y600A also showed more severe dominant effects than either DVMAT-wt or DVMAT-Δ3. We propose that these behavioral deficits result from the redistribution of DVMAT from SVs to LDCVs. By extension, our data suggest that the balance of amine release from SVs versus that from LDCVs is critical for the function of some aminergic circuits.

Key words: dopamine; LDCV; octopamine; serotonin; synaptic; vmat

Introduction

Neurons support at least two distinct mechanisms for the exocytosis of monoamine neurotransmitters including release by both synaptic vesicles (SVs) and large dense-core vesicles (LDCVs; Thureson-Klein, 1983; Kelly, 1993; Bruns and Jahn, 1995; Bruns et al., 2000; De-Miguel and Trueta, 2005; Südhof and Rizo, 2011). Only SVs are found at the active zone of the synapse, and they are thus required for neurotransmitter release into the synaptic cleft (Kelly, 1993; Südhof and Rizo, 2011). Unlike SVs, LDCVs contain peptide neurotransmitters and are extrasynaptically released from both the nerve terminal and somatodendritic sites (Kuffler et al., 1987; Kelly, 1993; Bruns and Jahn, 1995; Bruns et al., 2000). As such, LDCVs and related organelles may contribute more than SVs to the activation of extrasynaptic receptors, and to some of the behavioral effects of both psychostimulants and antidepressants (Kalivas and Duffy, 1993a,b; Blier et al., 1998; Adell et al.,

2002; Vezina, 2004; Li et al., 2005; Colgan et al., 2009; Richardson-Jones et al., 2010). However, the actual importance of amine release from SVs versus LDCVs or other vesicles for behavior and the function of the nervous system as a whole remains obscure, both in mammals and invertebrates. It also remains unclear whether sorting to each vesicle population differs across cell types.

Vesicular monoamine transporters (VMATs) are responsible for the storage of biogenic amines in both SVs and LDCVs (Eiden and Weihe, 2011; Blakely and Edwards, 2012; Lawal and Krantz, 2013). Some of the underlying signals and pathways regulating aminergic storage and release have been determined using *in vitro* assays and cultured cells (Tan et al., 1998; Waites et al., 2001; Yao et al., 2004; Li et al., 2005; Colgan et al., 2007; Yao and Hersh, 2007; for review, see Fei et al., 2008). It remains to be established how these signals might affect transporter trafficking and aminergic signaling *in vivo*. Importantly, the consequences of altering VMAT trafficking signals *in vivo* might reveal the relative significance of amine release via SVs versus that of LDCVs for specific behaviors and whether the balance of release from each type has functional relevance.

The model organism *Drosophila melanogaster* provides a powerful system with which to test the effects of VMAT trafficking mutants *in vivo* and thus to address questions of behavioral significance. To maximize our ability to detect phenotypic differences, we have focused on a relatively severe trafficking mutant: a deletion of the terminal 23 aa of the *Drosophila* vesicular monoamine transporter (DVMAT-Δ3). This deletion disrupts known and predicted endocytosis signals proposed to be required for both *de novo* trafficking and recycling to SVs following exocytosis at the synapse (Greer et al., 2005; Fei et al., 2008; Grygoruk et al., 2010). We also studied the effects of an alanine substitution mutant that more specifically disrupts a tyrosine-based sorting motif (Y$_{600}$XXY$_{603}$; Grygoruk et al., 2010). We find that both mutations retain the ability to sort to LDCVs, despite decreased sorting to SVs. Both appear to localize more to LDCVs than wild-type DVMAT, with Y600A paradoxically showing a more severe phenotype when expressed in an aminergic cell type. The behavioral phenotypes of these mutations suggest that the balance of DVMAT trafficking to SVs versus that to LDCVs is critical for the function of a subset of aminergic circuits and provides a model to explore differences in trafficking mechanisms across aminergic neurons versus non-aminergic neurons.

Materials and Methods

Generation and use of Drosophila transgenes and mutants

For insertion of the supereclyptic green fluorescent protein (GFP) pHluorin moiety into the lumenal loop of DVMAT, an XmaI(c|ccggg) site was first introduced into the cDNA construct pMT-DVMAT-A-HA sequence (Greer et al., 2005) using the Quikchange Site-Directed Mutagenesis Kit (Stratagene). cDNA representing the pHluorin moiety was inserted into the XmaI site to replace the HA tag, and the resultant fragment was ligated to sequence encoding, as follows: (1) the wt DVMAT C-terminal region; (2) the Y600A mutation; or (3) the Δ3 mutation. Each pHluorin-tagged DVMAT variant was subcloned into the pExp-upstream activator sequence (UAS) expression vector (Exelixis), followed by injection into the *white*[1118] strain (BestGene *Drosophila* Embryo Injection Services or Rainbow Transgenic Flies).

The null *dVMAT* allele *dVMAT*[P1] (Oh et al., 2003; Simon et al., 2009) and lines expressing both wild-type and mutant forms of HA-tagged *UAS-DVMAT* transgenic fly lines on chromosomes 2 and 3 have been described previously (Chang et al., 2006; Grygoruk et al., 2010). Note that all *UAS-DVMAT* transgenes used here encode the neuronal isoform of
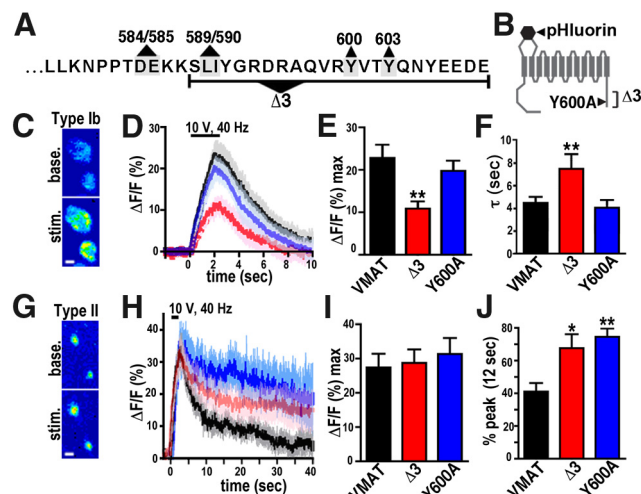
DVMAT (DVMAT-A); a distinct RNA splice variant, DVMAT-B, is expressed in a small subset of histamine-containing glia in the adult visual system (Romero-Calderón et al., 2008) and is not pertinent to the studies described here. The drivers *elav-Gal4* (Robinow and White, 1988), *da-Gal4* (Caudy et al., 1988), and *Tdc2-Gal4* (Cole et al., 2005) were used to express wild-type and trafficking mutant DVMAT constructs, as indicated in the text. Additional UAS lines that were used as markers included GFP-tagged versions of atrial natriuretic factor (ANF), syt1, Rab5, Rab7, Rab11, and lysosome-associated membrane protein (LAMP) proteins (Entchev et al., 2000; Rao et al., 2001; Wucherpfennig et al., 2003; Emery et al., 2005; Pulipparacharuvil et al., 2005; Akbar et al., 2009).

Live imaging of DVMAT-pHluorins

For imaging studies, third-instar larvae were dissected in chilled Ca^{2+}-free HL3.1 saline (70 NaCl, 5 mM KCl, 4 mM MgCl$_2$, 10 mM NaHCO$_3$, 5 mM trehalose, 115 mM sucrose, 5 mM HEPES; Feng et al., 2004) adjusted to pH 7.32. Measurements of exocytosis and endocytosis were performed in HL3.1 solution, pH 7.32, supplemented with 2.0 mM calcium (to allow normal rates of exocytosis and endocytosis) and 7 mM L-glutamic acid (LGA; Sigma; used to block muscle contraction for imaging). LGA and calcium were added to HL3.1 on the day of the experiment, and fresh stock solutions of LGA were made weekly. All images were acquired on a Zeiss Axio Examiner Z1 microscope using a cooled back-illuminated, electron-multiplying CCD camera (iXon3 897, Andor) and a DG4 light source (Sutter) with a GFP Brightline Filter Set (Semrock) and a Zeiss Achroplan water-immersion objective [100×, 1.0 numerical aperture (NA)]. The data acquisition rate for type Ib terminals was 20 images/s. For the longer time course of synaptic trafficking seen in type II terminals, data were acquired at 10 images/s. For quantification of exocytosis and endocytosis, individual boutons from muscle 13 in abdominal segment A4 were designated as regions of interest and tracked with the MeasureStack plugin in ImageJ (National Institutes of Health). Boutons that moved in or out of focus during image acquisition were discarded before analysis. Background fluorescence was subtracted from observed fluorescence to obtain a corrected value at each time point (F). To normalize for photobleaching, F at the onset of recording ($F_{initial}$) and during the following 20 s of each trace (before the stimulus) were used to fit a single exponential $F_{initial} e^{-kt}$, in which k is the time constant due to photo bleaching and t equals time. To further standardize the curves, F_{rest} was defined as the average F over a 2 s period immediately before the stimulus. The normalized F was then represented as $F(F_{initial} e^{-kt}/F_{rest})$. $\Delta F/F$ was calculated using the normalized F and the equation $(F - F_{baseline})/F_{baseline}$, where $F_{baseline}$ is the average of the 10 frames (0.5 s duration) before stimulus. Maximal $\Delta F/F$ was calculated as $(F_{peak} - F_{baseline})/F_{baseline}$, where F_{peak} is the average of the 10 frames during the 0.5 s after cessation of the 40 Hz stimulus. To quantify endocytosis rates in type Ib terminals, $\Delta F/F$ values over the first 30 s following the peak value at stimulus offset were fit to a single exponential using GraphPad Prism and the equation $Y = (Y_0 - Y_p)e^{-kt}$, where Y_0 represents the peak after the stimulus, Y_p represents the asymptotic plateau value of Y at $t = \infty$, and k is the rate constant of decay. Endocytosis rates are represented as the time constant $\tau = 1/k$. For type II terminals, $\Delta F/F$ was calculated as above for type Ib terminals. For some traces from type II boutons expressing the DVMAT-Y600A mutant (see text), we observed minimal decay during the recording period, thus prohibiting the calculation of a time constant. Therefore, to compare endocytosis across genotypes, we calculated the decrease in relative fluorescence ($\Delta F_{decrease}/F)_t$ at increasing times following the stimulus using the equation $\Delta F_t = (F_{peak} - F_t)/F_{baseline}$, where F_t in Figure 1 is the value at 10 s following the peak, or 12 s after the initial stimulus at time 0.

Immunofluorescent labeling

Larval brain plus ventral nerve cord or body wall fillets [used to visualize the neuromuscular junction (NMJ)] were prepared in PBS from wandering third-instar larvae. The fillet (including the larval brain plus nerve cord) or brain plus nerve cord alone were fixed in 4% paraformaldehyde (for 40 min at ambient temperature), washed in PBS (3×) and PBS-T (PBS and 0.1% Triton X-100 detergent), and incubated for 1 h at room temperature in PBS-T plus 5% normal goat serum (NGS; "blocking so-

A

584/585 589/590 600 603

...LLKNPPTDEKKSLIYGRDRAQVRYVTYQNYEEDE

Δ3

B pHluorin

Y600A Δ3

C Type Ib
base.
stim.

D 10 V, 40 Hz

E

F

G Type II
base.
stim.

H 10 V, 40 Hz

I

J

Figure 1. DVMAT mutants display slowed endocytosis at the larval NMJ. *A*, The DVMAT C terminus. The final 34 aa of the 39 aa cytosolic C-terminal domain of DVMAT are shown. The extent of the Δ3 deletion and the sites of the predicted dileucine motif (residues 589/590 in the DVMAT sequence), upstream acidic residues (584 – 585), and the tyrosine-based motif (Y600 and Y603) are indicated. *B*, The diagram represents the DVMAT protein, and shows the locations of the lumenal pHluorin insert and both the Δ3 deletion and the Y600A mutation within the cytosolic C terminus of DVMAT. *C*, False color images of type Ib terminals at baseline and following stimulation. Scale bar, 1 μm. *D*, Summed traces of DVMAT-wt (black, $n = 15$), DVMAT-Δ3 (red, $n = 9$), and DVMAT-Y600A (blue, $n = 8$) in type Ib terminals. Bar indicates 2 s stimulus (10 V, 40 Hz). *E*, Peak levels of exocytosis ($\Delta F/F$) were reduced in DVMAT-Δ3 relative to DVMAT-wt (VMAT); DVMAT-Y600A did not show a statistically significant difference from DVMAT-wt. For all panels: *$p < 0.05$, **$p < 0.01$, compared with DVMAT-wt by one-way ANOVA with Bonferroni post-test. *F*, The time constant for endocytosis (τ; see Materials and Methods) was elevated in DVMAT-Δ3 but not in DVMAT-Y600A compared with DVMAT-wt. *G*, False color images of type II terminals at baseline and following stimulation. Scale bar, 1 μm. *H*, Summed traces of DVMAT-wt (black, $n = 10$), DVMAT-Δ3 (red, $n = 9$), and DVMAT-Y600A (blue, $n = 8$) in type II terminals. Bar indicates 2 s stimulus (10 V, 40 Hz), as in *D*. (Note the difference in *x*- and *y*-axes in *H* vs *D*.) *I*, Peak levels of exocytosis (maximal$\Delta F/F$) for DVMAT-wt, DVMAT-Δ3, and DVMAT-Y600A did not detectably differ. *J*, Relative rates of endocytosis were calculated as the decay from peak $\Delta F/F$, measured at 12 s following the initial stimulus (10 s following the peak $\Delta F/F$; see Materials and Methods). Both DVMAT-Δ3 and DVMAT-Y600A differ from DVMAT-wt.

lution"). The blot was cut with a razor and appropriate sections incubated overnight in PBS-T and either 5% NGS and either mouse anti-HA (1:500; Covance) or rabbit anti-GFP primary antibodies (1:500; Invitrogen). After washing, preparations were incubated in the secondary antibodies goat anti-mouse Alexa Fluor 555 (1:1000; Jackson ImmunoResearch) and donkey anti-rabbit Alexa Fluor 488 (1:1000; Jackson ImmunoResearch) in PBS-T with 5% NGS. Washed brains were mounted onto slides using Aquamount solution (Thermo Scientific). Images were acquired using a Zeiss Plan-Apochromat 63× oil-immersion objective (1.4 NA) and a Zeiss 710 confocal scanning microscope.

Western blots
For Western blots of adult heads, 3- to 7-d-old adults were anesthetized using CO_2, and four heads (two males and two females) per genotype were homogenized in SDS-PAGE sample buffer. To prevent saturation, either a 1 or 0.5 head equivalent was used to quantify expression for one versus two copies of the driver plus the UAS transgene, respectively. Samples were loaded onto an 8% polyacrylamide gel, transferred to nitrocellulose, and probed overnight at 4°C with primary antibodies including mouse anti-HA.11 (1:1000–1:3000) to detect HA-tagged DVMAT transgenes, and mouse anti-β-tubulin (1:500–1:3000) as a loading control. Additional primary antibodies used for Western blot analysis of sucrose density gradient fractionation included an mAb directed against *Drosophila* cysteine string protein (CSP; 1:1000–1:2000; Developmental Studies Hybridoma Bank) as a marker for SVs (Zinsmaier et al., 1990; van de Goor et al., 1995), rabbit anti-ANF (1:3000–1:

4000; Peninsula Laboratories/Bachem) as a marker for LDCVs (Rao et al., 2001), and rabbit anti-GFP (1:10,000, Invitrogen) to detect GFP-fused Rab-5, Rab-7, Rab-11, and LAMP proteins (Entchev et al., 2000; Rao et al., 2001; Wucherpfennig et al., 2003; Emery et al., 2005; Pulipparacharuvil et al., 2005; Akbar et al., 2009).

All Western blots were probed with either anti-mouse (1:2000; Bio-Rad) or anti-rabbit (1:2000; GE Healthcare) horseradish peroxidase-conjugated secondary antibodies for 45 min at ambient temperature, followed by SuperSignal West Pico Luminol/Peroxide (Pierce) and exposure to Kodak Biomax Light Film.

Sucrose density gradient fractionation
For sucrose density gradient fractionation experiments, adult flies were frozen on dry ice, and heads were separated from bodies using wire mesh sieves. Heads were ground over dry ice using a mortar and pestle, and the resultant powder homogenized using Teflon on glass (900 rpm for 2 min) in ice-cold homogenization buffer containing 10 mM HEPES, 1 mM EGTA, 0.1 mM $MgCl_2$, pH 7.4, and a protease inhibitor mixture (Roche). The homogenate was centrifuged for 1 min at 10,000 × g, at 4°C, and the postnuclear supernatant was layered on a 20–55% sucrose gradient. Gradients were centrifuged for 12–16 h, at 4°C at 30,000 rpm in a Beckman SW41 rotor; 15 fractions were subsequently collected from the bottom of the pierced centrifugation tube and were analyzed by Western blot (see above); the amounts of each protein of interest were expressed as a percentage of their total immunoreactivity summed across all fractions of the gradient.

Neurochemical analysis
For HPLC analysis of dopamine (DA) levels, four fly heads (two males plus two females) were manually collected and homogenized in 0.1 M perchloric acid containing 0.1% EDTA using a glass micro-tissue grinder (Kontes, Kimble-Chase). Insoluble debris was sedimented by centrifugation for 1 min at 13,000 × g, and the supernatant was filtered through a Millipore MC cartridge (EMD Millipore). The filtrate was diluted 10-fold before analysis, and 5 μl of the diluted sample was analyzed using HPLC with electrochemical detection (Antec Leyden) using a mobile phase consisting of sodium acetate (75 mM), sodium dodecane sulfonate (0.75 mM), EDTA (10 mM), triethylamine (0.01%), acetonitrile (12%), methanol (12%), tetrahydrofuran (1%), pH 5.5, pumped at a rate of 200 μl/min (model LC-10AD, Shimadzu) through a 100 × 2 mm column (3 μm; Hypersil C18, Keystone Scientific), as described previously (Chang et al., 2006; Simon et al., 2009).

Behavioral analysis
Handling. All lines used for behavioral testing were outcrossed for five generations into *white[1118]CS[10]* (*w[1118]* outcrossed ≥10 times to *Canton-S*); we refer to this line as "w(CS)" in the text and use either these or *Canton-S* flies (referred to in the text as "CS") as controls, as indicated. Flies were raised on cornmeal-molasses agar media at 23–25°C and 20–40% humidity in a 12 h light/dark cycle.

As described in Connolly and Tully (1998) and Simon et al. (2006), all behavioral experiments used flies naive to the assay and were performed at the same time of the day, in a range of 3–5 h, to avoid variation in performance linked to circadian rhythm. All behavioral assays, except for fertility and conditional viability, were performed in the same dedicated room under constant temperature (25°C).

Conditional viability. To test the rescue of density-dependent lethality caused by the *dVMAT[P1]* mutant, virgin flies were collected under CO_2 anesthesia 0–5 d before mating. Virgin females (*dVMAT[P1]*/CyO, 70 flies per mating session) were incubated with males [~35 per mating session, *dVMAT[P1]*/CyO; da-Gal4, UAS-DVMAT-wt, UAS-DVMAT-Δ3, or UAS-DVMAT-Y600A (chromosome 3)/da-Gal4, UAS-wt, UAS-wt-Δ3, or UAS-wt-Y600A (chromosome 3)] for 3 d in bottles at 25°C. After 12 d, the number of progeny from each bottle was counted each day for 5 consecutive days, and the percentage of progeny homozygous for *dVMAT[P1]* (those that were phenotypically Cy^+) was compared with the number of homozygous progeny predicted by standard Mendelian ratios.

Larval locomotion. To generate larvae for locomotion assays, adults [10 males and females per mating session, *dVMAT[P1]*/CyO, Actin-GFP; da-Gal4/+, UAS-DVMAT-wt(3), UAS-DVMAT-Y600A(3), or UAS-

DVMAT-Δ3(3)] were mated for 2 d at ~25°C in egg-laying chambers containing standard cornmeal-molasses agar media. Third-instar larvae homozygous for dVMAT[P1] (and heterozygous for da-Gal4 and UAS-DVMAT-wt, UAS-DVMAT-Δ3, or UAS-DVMAT-Y600A) were selected for the absence of the GFP marker using a dissecting microscope fitted with excitation and emission filters to detect GFP fluorescence. For locomotion assays, third-instar larvae were allowed to acclimate for 1 min to a chamber (100 × 15 mm) containing 1.5% agar (dissolved in distilled water). Larval velocity was recorded for 120 s using a piA2400–17gm camera (Basler Vision Technologies) and the Multi-Worm Tracker software as described (Swierczek et al., 2011; Pizzo et al., 2013). All tested larvae were saved, and their genotypes were confirmed as adults.

Negative geotaxis in adults. For negative geotaxis behavior (startle-induced climbing), flies were collected 3–7 d before the experiment under cold anesthesia and were allowed to acclimate for 30 s to a choice-test apparatus (Benzer, 1967; Connolly and Tully, 1998) before testing. To stimulate the flies and initiate each experiment, the apparatus was tapped on a bench top three times, and the percentage of flies able to climb to the upper tube of a choice-test apparatus in 15 s (the time needed for ~80% of 4-d-old control flies to reach the top chamber) was recorded. Between 20 and 100 flies (3–7 d post-eclosion and naive to the assay) were used per data point; the number of flies did not affect performance (data not shown). Experiments were performed in the dark using a photo-safe red light.

Fertility. For fertility experiments, flies were collected under CO_2 anesthesia 0–5 d before mating. To test male fertility, one male candidate of the indicated genotype was mated with three white[1118]CS[10] virgin females in a vial at room temperature. To test female fertility, one virgin female candidate of the indicated genotype was mated with four white[1118]CS[10] males in a vial at room temperature. Twelve days after initial mating, parents were removed and candidates were scored as fertile if the vial contained at least one larva, pupa, or adult. To ensure that candidates survived long enough to mate, only vials containing at least one male and one female during the first and second day after initial mating were included in the analysis.

Egg laying. Four females of the indicated genotype were mated to six white[1118]CS[10] control males in a vial for 3 d. Mated flies were then passed into a new vial each day for 10 d, and the number of eggs laid was counted each day. To quantitate adult progeny, the number of eclosed flies was recorded for 10 consecutive days.

Results

Synaptic trafficking of wild-type and mutant DVMAT

We have previously generated mutations in the C-terminal trafficking domain of DVMAT (for sequence, see Fig. 1A,B) and have shown that both the Y600A and Δ3 mutations reduce endocytosis of DVMAT in non-neuronal S2 cells and in the neuronal cell line DmBG2C6 (Grygoruk et al., 2010). To determine the effect of these mutations on endocytosis at the nerve terminal *in vivo*, we generated wt and mutant DVMAT constructs containing a pH-sensitive variant of GFP, or pHluorin (Miesenböck et al., 1998) inserted into the lumenal loop of DVMAT-wt, DVMAT-Y600A, and DVMAT-Δ3 (at the same site for all three; Fig. 1B). Each construct was expressed *in vivo* as a UAS transgene, using the Gal4/UAS system (Brand and Perrimon, 1993). In the Gal4/UAS system, a transgenic "driver" containing a tissue-specific promoter from the fly is used to express the yeast transcription factor Gal4. Binding of the Gal4 protein to a yeast UAS allows tissue-specific expression of the cDNA downstream of the UAS sequence (Brand and Perrimon, 1993; St Johnston, 2013). Type Ib terminals at the *Drosophila* NMJ have been well characterized as a model to study vesicle release and recycling using both electrophysiological and live-imaging techniques (Budnik et al., 2006; Davis, 2006; Collins and DiAntonio, 2007; Levitan, 2008). To drive the expression of each variant at this site, we used the *elav-Gal4* driver (Robinow and White, 1988). To quantify exocy-

tosis for each line, we measured the peak fluorescence signal following stimulation, normalized to baseline fluorescence (Miesenböck et al., 1998; Sankaranarayanan et al., 2000; Dreosti and Lagnado, 2011). The peak $\Delta F/F$ for DVMAT-Δ3 (shown in red) was significantly lower than that for DVMAT-wt (shown in black) in type Ib terminals (Fig. 1D), suggesting that the relative level of exocytosis was reduced. The peak $\Delta F/F$ for DVMAT-Y600A (shown in blue) did not statistically differ from that of DVMAT-wt. Additional experiments using bafilomycin to block reacidification of the endocytosing vesicles confirmed that the observed defect in DVMAT-Δ3 exocytosis cannot be explained by increased endocytosis (data not shown). To specifically quantify the rates of endocytosis, we fit a single exponential to the declining phase of the curve beginning immediately after the peak until 30 s after the peak. We find that the time constant (τ) for DVMAT-Δ3 is higher than that for either DVMAT-wt or DVMAT-Y600A, indicating a slower rate of endocytosis for the Δ3 mutant (Fig. 1F). The amount of each DVMAT-pHluorin variant present at the nerve terminal was quantified using both absolute fluorescence at baseline and following alkalinization with the membrane-permeant base NH_4Cl, using the latter to reveal the total content of acid-sensitive pHluorins (data not shown; Sankaranarayanan et al., 2000). Since levels of the Δ3 construct did not exceed those of either wt or Y600A, the decrease in the endocytic rate of the Δ3 pHluorin relative to wt and Y600A is unlikely to be due to saturation of the endocytic machinery. Overall, these data demonstrate that, at type Ib terminals, motifs contained within the region defined by the Δ3 deletion are required for efficient exocytosis and endocytosis, and that the Y600A mutant has little effect on either the extent of exocytosis or the rate of endocytosis at this terminal type.

To determine how these mutations would affect trafficking at an aminergic synapse, we used *Tdc2-Gal4* to express *UAS-DVMAT* transgenes at type II terminals, which store and release octopamine (Monastirioti et al., 1995; Vömel and Wegener, 2008). Tyrosine decarboxylase 2 (Tdc2) is the neuronal isoform of the first enzyme in the biosynthetic pathway for the neurotransmitters tyramine and octopamine, the latter both structurally and functionally similar to mammalian norepinephrine (Cole et al., 2005; Roeder, 2005). Flies also synthesize dopamine, but through a different pathway that is identical to mammals, and includes the enzymes tyrosine hydroxylase and dopa decarboxylase (Hirsh and Davidson, 1981; Neckameyer and White, 1993; Birman et al., 1994; Wright, 1996; Monastirioti, 1999). Using the same stimulus protocol as for type Ib terminals, we did not detect a difference in the maximal $\Delta F/F$ during exocytosis among DVMAT-wt, DVMAT-Δ3, and DVMAT-Y600A (Fig. 1H,I). By contrast, the decrease in fluorescence following the stimulus was impaired for both DVMAT-Δ3 and DVMAT-Y600A (Fig. 1H,J), indicating an endocytic defect for both DVMAT trafficking mutants in octopaminergic nerve terminals. Endocytosis of both wt and mutant DVMAT was generally slower in type II versus type Ib terminals, as suggested previously for mammalian aminergic versus non-aminergic neurons in culture (Onoa et al., 2010). Differences in the overall rate of endocytosis as well as the effects of the Y600A mutation suggest potential differences in the trafficking machinery at type Ib versus type II terminals.

Immunofluorescent localization of wt and mutant DVMAT

To determine the baseline, subcellular localization of wt and mutant DVMAT, we performed immunofluorescent labelings. We used the driver *Tdc2-Gal4* to express the transgenes in octopaminergic and tyraminergic cells and focused on midline octo-

paminergic neurons in the larval ventral nerve cord. The somata of these cells are easily visualized, and their processes form the type II terminals at the NMJ (Monastirioti et al., 1995; Vömel and Wegener, 2008). To label SVs at the NMJ, we used the marker *UAS-Syt1-GFP* and an antibody to GFP (Zhang et al., 2002). Both wild-type and mutant forms of DVMAT partially colocalized with Syt1 (Fig. 2A–I), confirming that all three should, to some extent, target to secretory vesicles at the nerve terminal. These data are consistent with our results using pHluorin-tagged DV-MATs, which showed that both wt and mutant forms can undergo exocytosis to some degree.

Importantly, octopaminergic neurons contain approximately equal numbers of LDCVs and SVs (Atwood et al., 1993). To confirm that, similar to mammalian forms of VMAT, DVMAT also localizes to LDCVs, we performed additional labelings, using a transgene encoding a chimera of ANF fused to GFP (*UAS-ANF-GFP*) as a marker for LDCVs (Rao et al., 2001; Wong et al., 2012). Using a primary antibody to GFP (Rao et al., 2001), labeling was detected both in the nerve terminals (data not shown) and the somata, where individual puncta could be distinguished more clearly (Fig. 2J–R). DVMAT-wt colocalizes extensively with ANF-GFP (Fig. 2L), as expected from previous studies demonstrating that mammalian VMAT orthologs sort to LDCVs as well as SVs and, indeed, may preferentially sort to LDCVs (Liu et al., 1994; Nirenberg et al., 1997; Li et al., 2005). Both DVMAT-Y600A and DVMAT-Δ3 showed extensive colocalization with the ANF-GFP marker similar to wt DVMAT, suggesting that, despite the absence of several predicted sorting motifs in the Δ3 mutant, both Δ3 and Y600A are capable of sorting to LDCVs as well as SVs.

Subcellular fractionation of DVMAT to SVs and LDCVs
To quantitate the relative distribution of wt and mutant DVMATs to SVs versus LDCVs, we performed sucrose density fractionation of adult head homogenates. Unlike the glycerol velocity gradients we used previously to measure DVMAT trafficking to SVs, sucrose density gradients can resolve LDCVs as well as SVs (Liu et al., 1994; Varoqui and Erickson, 1998). The *UAS-ANF-GFP* transgene (Rao et al., 2001; Wong et al., 2012) and CSP (Zinsmaier et al., 1990) were used to track the sedimentation of LDCVs and SVs, respectively. Since the *ANF-GFP* transgene has been used primarily for imaging experiments rather than biochemical studies (Rao et al., 2001; Wong et al., 2012), we performed additional control experiments using markers for other organelles (Fig. 3). We find that both the CSP and ANF-GFP sedimentation profiles are distinct from those of markers for early endosomes (rab5), late endosomes (rab7), the sorting endosome (rab11), and lysosomes (i.e., LAMPs; Entchev et al., 2000; Rao et al., 2001; Wucherpfennig et al., 2003; Emery et al., 2005; Pulipparacharuvil et al., 2005; Akbar et al., 2009; Fig. 3A–E). These data demonstrate the specificity of the ANF and CSP markers for determining the relative localization of wt and mutant forms of DVMAT to both SVs and LDCVs in sucrose gradients.

To detect DVMAT in gradient fractions, we used an mAb to the HA epitope tag common to each variant (Greer et al., 2005; Grygoruk et al., 2010). For the experiments shown in Figure 4, the pan-neuronal driver *elav-Gal4* was used to express the *UAS-DVMAT* transgenes in the *dVMAT* wt background. We find that the relative amounts of both DVMAT-Δ3 (Fig. 4B,E) and DVMAT-Y600A (Fig. 4C,F) that co-sediment with the SV marker CSP are less than that observed for wt DVMAT (Fig. 4A,D). These results are consistent with and expand on our pre-
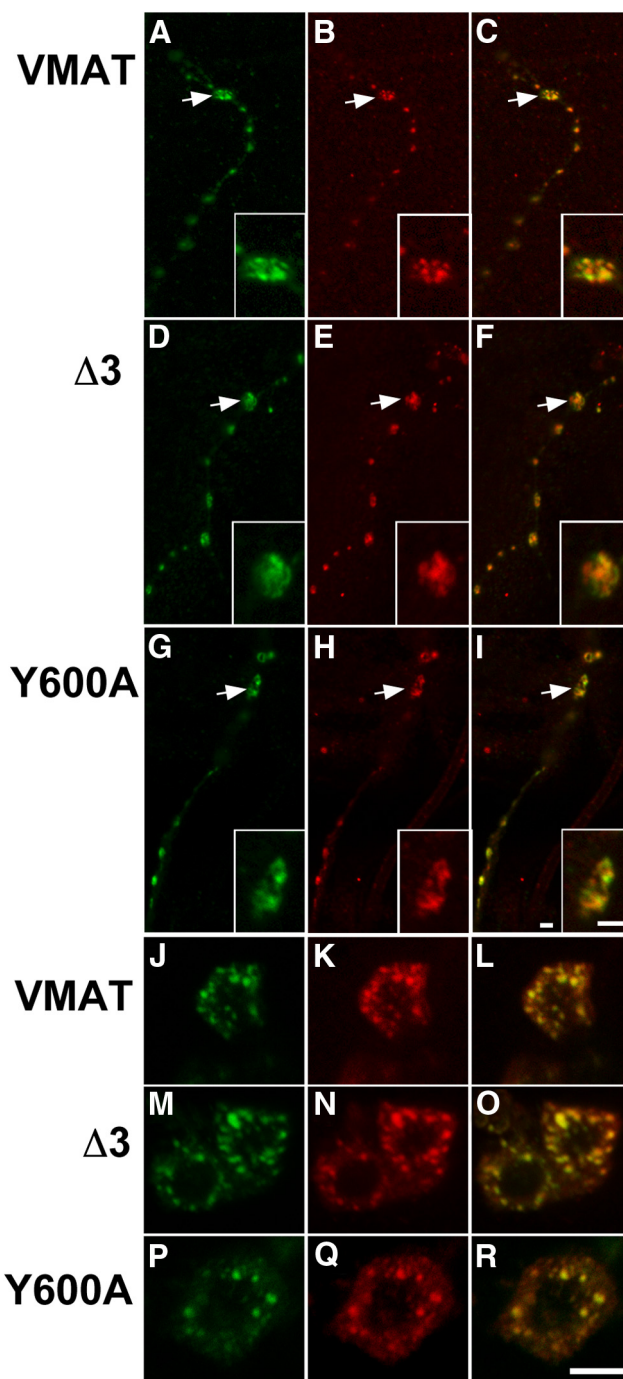
Figure 2. Immunolabeling of wt and mutant DVMAT. *A–R*, The *Tdc2-Gal4* driver was used to express the HA-tagged *UAS-DVMAT* transgenes encoding DVMAT-wt (*A–C, J–L*), DVMAT-Δ3 (*D–F, M–O*), and DVMAT-Y600A (*G–I, P–R*) with either *UAS-syt1-GFP* (*A–I*) or *UAS-ANF-GFP* (*J–R*) as markers for SVs or LDCVs, respectively. Body wall fillets containing type II NMJ terminals expressing the transgenes (*A–I*) or larval nerve cords (*J–R*) were colabeled with a monoclonal antibody to the HA tag in DVMAT and an antiserum to GFP to detect either syt1-GFP or ANF-GFP, followed by the appropriate secondary antibodies to label DVMAT red and the markers green. Processes on either muscle 7 or 13 were used to visualize expression in type II nerve terminals in *A–I*. Scale bars: (in *I*) *A–I*, 2 μm; (in *R*) *J–R*, 5 μm.

vious results using other fractionation techniques (Grygoruk et al., 2010). In addition, we find an additional peak for DVMAT-Δ3 near the center of the gradient at a position distinct from either CSP or ANF-GFP, suggesting that some portion of Δ3 is ectopically localized when expressed using the pan-neuronal
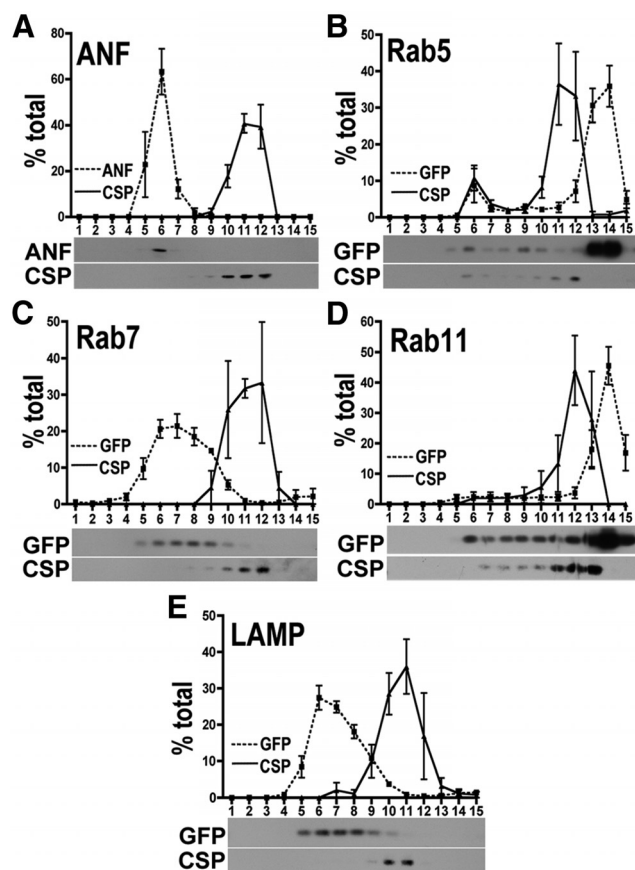
Figure 3. Migration of markers on sucrose density gradients. **A–E**, Postnuclear homogenates from adult fly heads expressing ANF-GFP (**A**), Rab5-GFP (**B**), Rab7-GFP (**C**), Rab11-GFP (**D**), or LAMP-GFP (**E**) using the pan-neuronal driver *elav-Gal4* were separated by sucrose density gradient centrifugation and fractions probed on Western blots using primary antibodies to CSP (**A–E**) and either ANF (**A**) or GFP (**B–E**). The top of each panel shows the quantitation of three gradients for each marker. The bottom of each panel shows one of the three Western blots used for quantitation. The sedimentation pattern for rab5, rab7, and rab11, and LAMP markers differ from either CSP or ANF. For all panels, fraction 1 is the bottom of the gradient and fraction 15 is the top.

paminergic cells, contain large numbers of LDCVs as well SVs, we reasoned that expression in this cell type might afford a more accurate assessment of sorting DVMAT to LDCVs than pan-neuronal expression using *elav-Gal4*. Indeed, in contrast to the pattern seen using the *elav-Gal4* driver (Fig. 4), when expressed in octopaminergic and tyraminergic neurons, DVMAT-wt is more evenly distributed between the two distinct peaks that correspond to heavy fractions containing LDCVs and light fractions containing SVs (Fig. 5A,B). Both DVMAT-Y600A and DVMAT-Δ3 show decreased cosedimentation with the SV marker CSP in these gradients (Fig. 5A–C), which is consistent with the results of pan-neuronal expression shown in Figure 4 and the results of previously reported glycerol gradients (Grygoruk et al., 2010). However, in contrast to our results using *elav-Gal4*, when expressed in octopaminergic neurons using *Tdc2-Gal4*, DVMAT-Δ3 did not show a pronounced ectopic peak in the center of the gradient (Fig. 5A,B). Rather, sedimentation of DVMAT-Δ3 was increased in LDCV-containing fractions relative to DVMAT-wt (Fig. 5A,B,D). Surprisingly, DVMAT-Y600A showed an even more dramatic shift away from SVs compared with DVMAT-Δ3 (Fig. 5A,B,D). In summary, these results confirm than DVMAT-Δ3 and DVMAT-Y600A localize to SVs less than DVMAT-wt, but do not appear to show a decreased localization to LDCVs. Indeed, both mutants localize to LDCVs more than DVMAT-wt, especially when expressed in aminergic cells, which contain large numbers of LDCVs relative to most neurons. Comparison to the sedimentation patterns of other markers (Fig. 3) as well as immunolabeling (Fig. 2) reinforces the interpretation that the mutants localize to LDCVs rather than to an ectopic compartment in aminergic cells.

Functional effects of altered DVMAT trafficking

To determine how these trafficking defects might affect amine storage and amine-dependent behaviors, we compared the ability of *DVMAT-wt*, *DVMAT-Y600A*, and *DVMAT-Δ3* transgenes to rescue a null allele (*dVMAT^P1*) of the endogenous *dVMAT* gene (Simon et al., 2009). Transgenic flies were generated that express each one of the DVMAT variants in the *dVMAT^P1* mutant background. For each *UAS-DVMAT* variant, we used two independent insertions, one on the second and one on the third chromosome. We then generated lines expressing one or two copies of each insertion coupled with one or two copies of each driver, respectively. For initial rescue experiments, we used the broadly expressed driver *daughterless-Gal4* (*da-Gal4*), as previously described (Simon et al., 2009). To assess DVMAT protein expression in each transgenic line, we used Western blots of adult head homogenates probed with a primary antibody to the HA epitope tag inserted in each *DVMAT* transgene (Fig. 6A,B). Expression levels across independent insertions and between wt and mutant transgenes were similar using comparable copy numbers of each transgene (Fig. 6A,B). Note that some lines showing high expression levels of DVMAT-Y600A rarely survived, resulting in the absence of a lane representing two copies of *UAS-DVMAT-Y600A* on the third chromosome (Fig. 6B).

To determine whether mutant forms of DVMAT could rescue amine storage, we performed HPLC analysis with electrochemical detection. The mouse VMAT2 knockout and the *dVMAT* null mutant show dramatic reductions in tissue monoamine content (Fon et al., 1997; Simon et al., 2009). Consistent with these data, we see a reduction in dopamine content in the adult heads of the *dVMAT^P1* null mutant compared with the CS control (Simon et al., 2009). The content of tissue DA in flies rescued with one copy

driver *elav-Gal4* (Fig. 4B,E). When compared with the profiles for other markers (Fig. 3), these data suggest that a portion of DVMAT-Δ3 may be redistributed to either late endosomes or lysosomes when broadly expressed in all neurons using *elav-Gal4*.

DVMAT-Y600A showed a distinct profile on sucrose gradients, marked by a second peak of immunoreactivity that overlapped with ANF-GFP (Fig. 4C,F). Consistent with previous data, the relative amounts of both DVMAT-Δ3 and DVMAT-Y600A in peak fractions containing SVs was less than that of DVMAT-wt (Fig. 4G). Conversely, the relative amounts of both DVMAT-Δ3 and DVMAT-Y600A in peak fractions containing LDCVs was not reduced and appeared elevated relative to that of DVMAT-wt (Fig. 4H), although the relatively small amount of protein in dense fractions made this difficult to assess. Nonetheless, this observation suggested that, in contrast to the deficit seen in sorting to SVs, trafficking of the mutants to LDVCs might be intact or elevated relative to DVMAT-wt.
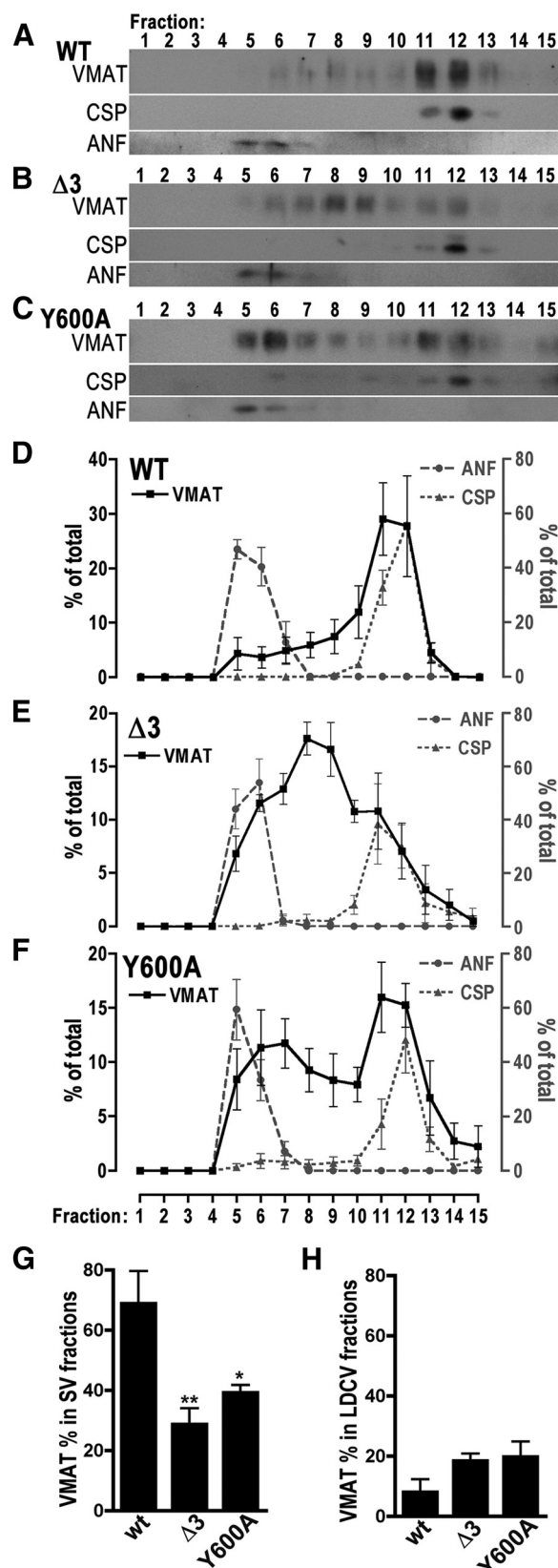
To further test that mutant transporters sort well to LDVCs and to more specifically assess the effects of the Δ3 and Y600A mutations in aminergic cells, we used the driver *Tdc2-Gal4* to express the *UAS-DVMAT* transgenes in octopaminergic and tyraminergic neurons (Fig. 5; again in the *dVMAT* wt background, as in Fig. 4). Since aminergic neurons, and in particular octo-

of either the *DVMAT-Δ3* or the *DVMAT-Y600A* mutation were indistinguishable from those rescued with one copy of *DVMAT-wt* (Fig. 6C). Similarly, rescue using two copies of *DVMAT-Δ3* yielded similar DA levels as rescue using two copies of the wt *DVMAT* transgene (Fig. 6D; two copies of *UAS-Y600A-3* were lethal; see Discussion). These results indicate that, despite defects in trafficking and potential differences in subcellular storage sites, both of the DVMAT mutants were able to store amines at levels similar to that in the wild-type transgene. Furthermore, since the mutants clearly support vesicular mono-amine storage *in vivo*, differential effects in behavioral rescue are likely to be caused by other defects, such as trafficking, that distinguish mutant from wt DVMAT.

Genetic rescue using a broadly expressed driver reveals circumscribed deficits for DVMAT-Δ3

We used genetic rescue to test the ability of wt and mutant DVMAT to improve the behavioral phenotypes caused by mutation of the endogenous *dVMAT* gene. For the loss-of-function background, we again used the P element insertion ($dVMAT^{P1}$) allele that does not express detectable levels of DVMAT protein and also behaves genetically as a null allele (Simon et al., 2009). $dVMAT^{P1}$ shows marked defects in a number of amine-dependent behaviors, including density-dependent survival, larval locomotion, adult climbing (negative geotaxis), and both male and female fertility (Simon et al., 2009; Chen et al., 2013). When expressed broadly using *da-Gal4*, many of the behavioral defects seen in the $dVMAT^{P1}$ null were similarly rescued by *DVMAT-wt*, *DVMAT-Y600A*, and *DVMAT-Δ3*, including measures of survival (Fig. 7A), adult negative geotaxis (Fig. 7B), larval locomotion (Fig. 7C), and male fertility (Fig. 7D). However, unlike *DVMAT-Y600A* and *DVMAT-wt*, *DVMAT-Δ3* failed to rescue female fertility under the same conditions (Fig. 8A). We confirmed the effects of *DVMAT-Δ3* on fertility using an additional independent *UAS* insertion line (Fig. 8C). To rule out the possibility that the failure of Δ3 to rescue female fertility was simply the result of inadequate expression, we repeated these assays using two copies of each *UAS-DVMAT-Δ3* transgene and two copies of the *da-Gal4* driver (Fig. 8B,D). Higher levels of DVMAT-Δ3 expression using the *da-Gal4* driver did not increase its ability to rescue female fertility. Indeed, high gene dosage of all three transgenes decreased their ability to rescue female fertility (Fig. 8B,D) compared with lower gene dosage (Fig. 8A,C). Homozygosity of the *UAS-DVMAT* transgenes in the absence of the driver did not decrease fertility, and it is, therefore, unlikely that spurious "floating" recessive mutations are responsible for this effect (data not shown). This result is consistent with previous data showing deleterious effects from high levels of DVMAT-wt overexpression (Chang et al., 2006). Together, these data indicate

←

and ANF as a marker for LDCVs, as indicated. *A–C* show representative Western blots, and *D–F* show quantitation of immunoblots for HA-DVMAT (solid black line), CSP (dotted gray line), and ANF (dashed gray line) for DVMAT-wt (*E*) DVMAT-Δ3 (*D*), and DVMAT-Y600A (*F*; n = 3–4 gradients per genotype; 2000–4000 flies per gradient). Whereas the major peak of DVMAT-wt is in SV fractions, DVMAT-Y600A shows a bimodal distribution in both light and heavy fractions that partially overlap with markers for SVs and LDCVs. The major peak of DVMAT-Δ3 differs from that of either CSP or ANF-GFP. Note that the scale on the left-hand axes differs for *D* vs *E* and *F*. *G*, *H*, The amount of each DVMAT isoform in fractions containing LDCVs (*G*, fractions 5 and 6) or SVs (*H*, fractions 10–12) was totaled. Total anti-HA immunoreactivity representing DVMAT differed between genotypes for SV-containing fractions (*G*, ANOVA, $p = 0.01$, Dunnett's multiple-comparison test vs wt, *$p < 0.05$ or **$p < 0.01$, as indicated) but not LDCV-containing fractions (*H*).

Figure 4. Sucrose density gradients of pan-neuronally expressed wt and mutant DVMAT. *A–F*, Postnuclear homogenates from fly heads expressing *UAS-DVMAT-wt* (*A*, *D*), *UAS-DVMAT-Δ3* (*B*, *E*), or *UAS-DVMAT-Y600A* (*C*, *F*) were separated by sucrose density gradient fractionation. Transgenes were expressed using the *elav-Gal4* driver in the *dVMAT* wt background and were coexpressed with *UAS-ANF-GFP*. Fractions were probed for DVMAT on Western blots using antibodies to the HA tag common to all DVMAT transgenes, CSP as a marker for SVs,
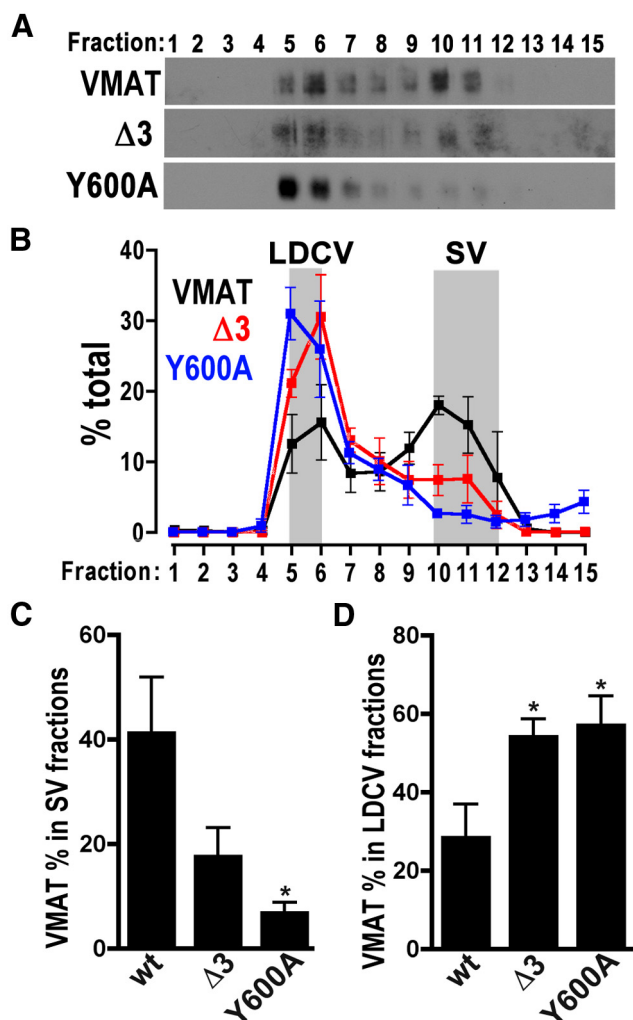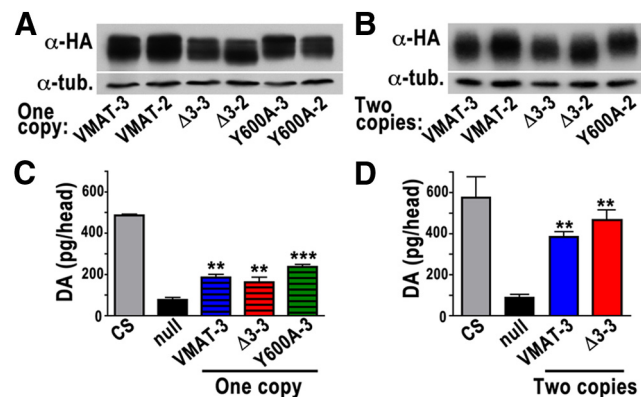
Figure 5. Sucrose density gradients of wt and mutant DVMAT expressed in octopaminergic neurons. **A**, Representative Western blots show sucrose gradients of homogenates from fly heads expressing DVMAT-wt, DVMAT-Δ3, or DVMAT-Y600A, as indicated, using the *Tdc2-Gal4* driver. **B**, Quantification of immunoblots (*n* = 3–5 per genotype) for DVMAT-wt, DVMAT-Δ3, and DVMAT-Y600A, as indicated. Compared with that of DVMAT-wt, HA immunoreactivity representing DVMAT-Δ3 and DVMAT-Y600A is shifted to fractions that contain LDCVs. Shaded bars show the position of markers for SVs and LDCVs. **C, D**, Total immunoreactivity representing DVMAT differed between genotypes for SV-containing fractions (**C**, ANOVA, *p* = 0.035, Dunnett's multiple-comparison test vs wt, **p* < 0.05) and LDCV-containing fractions (**D**, ANOVA, *p* = 0.03, Dunnett's multiple-comparison test vs wt, **p* < 0.05, as indicated).

Figure 6. Protein expression and rescue of amine levels by DVMAT trafficking mutants. **A, B**, Western blots probed with an antibody to the HA epitope tag in all DVMAT isoforms show DVMAT protein expression in *dVMAT*[P1] null flies expressing one copy (**A**) or two copies (**B**) of *UAS-DVMAT-wt, UAS-DVMAT-Δ3*, or *UAS-DVMAT-Y600A* transgenes coupled with either one copy (**A**) or two copies (**B**) of the *da-Gal4* driver, respectively. For *UAS-DVMAT-wt, UAS-DVMAT-Δ3*, and *UAS-DVMAT-Y600A*, independent insertions on both the second chromosome (VMAT-2, VMAT-Δ3–2, and VMAT-Y600A-2) and third chromosomes (VMAT-3, VMAT-Δ3–3, and VMAT-Y600A-3) are shown. Tubulin ("tub.") was used as a loading control (bottom panels). **C, D**, HPLC with electrochemical detection was used to measure dopamine levels in heads of control CS flies, the *dVMAT*[P1] null (null), and *dVMAT*[P1] rescued with either one copy (**C**) or two copies (**D**) of wt or mutant *UAS-DVMAT* transgenes on chromosome 3. The *dVMAT*[P1] null showed reduced levels of dopamine compared with *CS* controls. DA levels were partially rescued with one copy of *UAS-DVMAT-wt, UAS-DVMAT-Δ3*, or *UAS-DVMAT-Y600A* (all on chromosome 3), and were rescued to near wt levels with two copies of *UAS-DVMAT-wt* or *UAS-DVMAT-Δ3* and two copies of driver (two copies of *UAS-DVMAT-Y600A* were lethal; mean ± SEM, one-way ANOVA, *p* < 0.0001, *n* = 3–5 per genotype. Bonferroni post-test, ****p* < 0.001 between null and Y600A in **C** and ***p* < 0.01 between null and all other lines in **C** and **D**).

are particularly sensitive to changes in DVMAT trafficking, and that this is most likely the cause of female infertility.

Rescue using a specific aminergic driver reveals behavioral defects for DVMAT-Y600A

To more specifically assess the functional effects of the DVMAT trafficking mutants in aminergic cells, we performed rescue experiments using the *Tdc2-Gal4* driver (Fig. 9; Cole et al., 2005). *Tdc2-Gal2* was used rather than other aminergic drivers because the expression of wild-type DVMAT in octopaminergic and tyraminergic neurons using *Tdc2-Gal2* rescued the *dVMAT*[P1] deficits in survival, larval locomotion, and female fertility (Chen et al., 2013). By contrast, the expression of wt DVMAT in either serotonergic or dopaminergic neurons (or both) had little or no effect on these behaviors (Chen et al., 2013).

As shown in Figure 9, *A* and *B*, the expression of DVMAT-wt, DVMAT-Δ3, and DVMAT-Y600A using the *Tdc2-Gal4* driver each rescued the male fertility defect of *dVMAT*[P1]. In addition, the expression of DVMAT-wt using the *Tdc2-Gal4* driver rescued the female fertility defect of *dVMAT*[P1], albeit to levels less than w(CS) controls (Fig. 9C). Similar to our results with *da-Gal4* (Fig. 8C), using *Tdc2-Gal4* to express the *UAS-DVMAT-Δ3* transgene failed to rescue female fertility (Fig. 9C). However, in contrast to our experiments with *da-Gal4*, using *Tdc2-Gal4* to express *UAS-DVMAT-Y600A* also failed to rescue female fertility (Fig. 9C). For DVMAT-wt and DVMAT-Δ3, higher expression using two copies of *Tdc2-Gal4* and two *UAS–DVMAT* transgenes yielded results similar to those obtained using one copy (Fig. 9D). The expression of two copies of *UAS-DVMAT-Y600A* with two copies of *Tdc2-Gal4* was lethal in the *dVMAT*[P1] null background, thus preventing male or female fertility assays in Figure 9, *B* or *D*, respectively. In addition, the rescue of baseline larval locomotion

that the circuits that regulate female fertility are more sensitive to the effects of the DVMAT-Δ3 trafficking mutation and that this effect is not simply a result of insufficient expression.

Female fertility has been previously shown to be dependent on circuits that promote egg laying (Monastirioti et al., 1996; Lee et al., 2003; Monastirioti, 2003; Lee et al., 2009). Importantly, these circuits do not regulate development, but rather allow mature eggs to pass out of the ovary and through the oviduct (Monastirioti et al., 1996; Lee et al., 2003; Monastirioti, 2003; Lee et al., 2009). The *dVMAT* mutant phenotype includes defects in egg retention and egg laying, which can be partially rescued using the wt DVMAT transgene as well as DVMAT-Y600A (Fig. 8*E,F*). By contrast, the expression of DVMAT-Δ3 failed to rescue egg laying (Fig. 8*E,F*) or the similar metric of the number of progeny per female (data not shown). These data suggest that the aminergic circuits that innervate the ovary and oviduct and allow egg laying
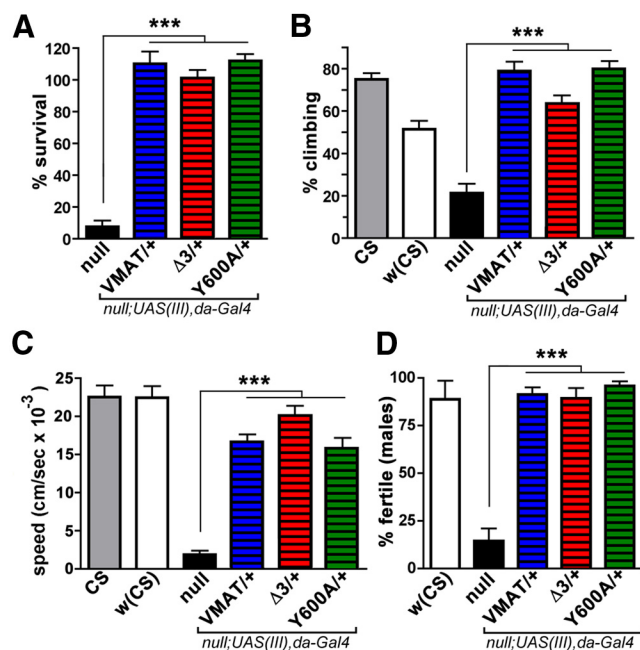
Figure 7. Multiple aspects of the *dVMAT* mutant phenotype are rescued by DVMAT trafficking mutants. ***A–D***, One copy of the broadly expressed driver *da-Gal4* (chromosome 3) was used to express one copy (chromosome 3) of *UAS-DVMAT-wt* (VMAT), *UAS-DVMAT-Δ3* (Δ3), or *UAS-DVMAT-Y600A* (Y600A) in the *dVMAT^P1* (null) background. Control flies used for each test were either *CS* or *w^1118CS_10* [indicated as w(CS)] or both as indicated. Each genotype was tested for its ability to rescue specific aspects of the *dVMAT^P1* mutant phenotype. We did not detect statistically significant differences in the ability of *DVMAT-wt* vs mutant transgenes to rescue: density-dependent lethality (*n* = 5 experiments for all genotypes; ***A***); the adult startle and climbing response (negative geotaxis, *n* ≥ 13 per genotype; ***B***); larval locomotion (*n* ≥ 19 larvae per genotype; ***C***); or male fertility (*n* ≥ 44 crosses per genotype; ***D***). Histograms show the mean ± SEM; one-way ANOVA, *p* < 0.0001 for all panels; Bonferroni post-test, ****p* < 0.001, as indicated.

using DVMAT-Y600A was less effective than rescue using either DVMAT-wt or DVMAT-Δ3 (Fig. 9E). Thus, similar to the trafficking phenotype of Y600A (Fig. 5), the behavioral phenotype of Y600A appeared to be more severe when it was specifically expressed in aminergic neurons.

DVMAT-Y600A behaves as a dominant allele

At comparable levels of expression, DVMAT-Y600A appeared to be more deleterious than either wt or Δ3. In addition to the negative effects of the higher gene dosage effect seen for larval locomotion in Figure 9E, we were unable to obtain adults for some of the experiments shown in Figures 6, 8, or 9 using *da-Gal4* or *Tdc2-Gal4* to express two copies of Y600A. We hypothesized that these observations might reflect a more severe dominant effect of the Y600A mutation that was different from that of either DVMAT-wt or DVMAT-Δ3. To more specifically compare the potential dominant effects of each allele, we expressed the DVMAT transgenes in the wt *dVMAT^+* rather than the *dVMAT^P1* loss-of-function background (Fig. 10A–D). Using two copies of *Tdc2-Gal4* and two copies of each *UAS-DVMAT* transgene, we did not observe a marked difference in larval locomotion or male fertility with DVMAT-Y600A overexpression compared with DVMAT-wt (Fig. 10A,B). By contrast, overexpression of DVMAT-Y600A with the *Tdc2-Gal4* driver caused a pronounced decrease in both female fertility (Fig. 10C) and the number of progeny per female (Fig. 10D) under conditions in which the overexpression of DVMAT-wt and DVMAT-Δ3 did not show detectable defects. We conclude that, for some behav-
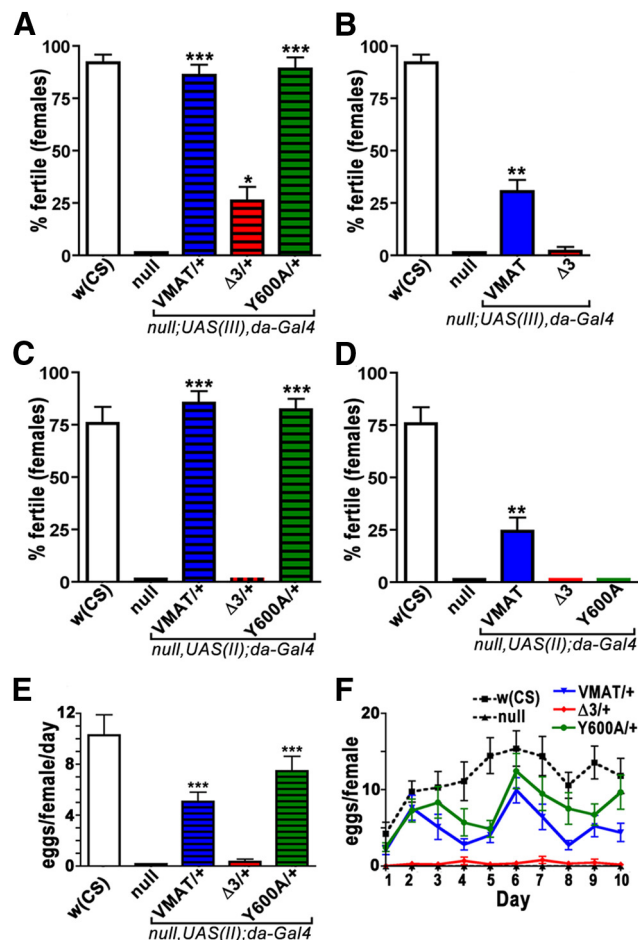

Figure 8. Female fertility and egg laying is compromised by DVMAT-Δ3. ***A–D***, Potential rescue of the *dVMAT^P1* mutant defect in female fertility was tested using one copy of the indicated *DVMAT* transgene and one copy of the *da-Gal4* driver (***A***, ***C***) or two copies of both the indicated *DVMAT* transgene and *da-Gal4* driver (***B***, ***D***). Insertion sites for the UAS transgenes were on either chromosome 3 (***A***, ***B***) or chromosome 2 (***C***, ***D***). One copy of either *DVMAT-wt* or *DVMAT-Y600A* on the third (***A***) or second chromosomes (***C***) rescued female fertility to control w(CS) levels; the *DVMAT-Δ3* insertions on the second and third chromosomes did not rescue female fertility. ***B***, ***D***, Fertility defects were observed for flies expressing two copies of *DVMAT-wt*, *DVMAT-Y600A*, or *DVMAT-Δ3* with two copies of the *da-Gal4* driver. Columns in ***A–D*** indicate the average percentage of crosses yielding any progeny, mean ± SEM, *n* = 41–69 vials per genotype; one-way ANOVA, *p* < 0.0001 for all panels; Bonferroni post-test, **p* < 0.05, ***p* < 0.01, or ****p* < 0.001, as indicated between null and rescue lines. ***E***, ***F***, Egg laying. Shown are the average number of eggs laid (mean ± SEM) per female (fecundity) for *dVMAT^P1* nulls rescued with one copy of *UAS-DVMAT-wt*, *UAS-DVMAT-Y600A*, and *UAS-DVMAT-Δ3*, and one copy of *da-Gal4*. Each set of mating sessions was scored for 10 d and is displayed as either the overall average across all 10 d (***E***) or the number of eggs for each day of the testing period (***F***). The number of eggs laid for w(CS) controls is also shown. *dVMAT^P1* null females (null) are essentially unable to lay eggs. This defect is partially rescued using one copy of *UAS-DVMAT-wt* or *UAS-DVMAT-Y600A*, but not *UAS-DVMAT-Δ3*. One-way ANOVA, *p* < 0.0001; Bonferroni post-test, ****p* < 0.001 as indicated compared with *dVMAT^P1* null; *n* = 18–26 vials per genotype.

iors, DVMAT-Y600A can exert a genetically dominant effect that is distinct from either the "hypermorphic" effects of overexpressing DVMAT-wt or the partial loss-of-function ("hypomorphic") effects of DVMAT-Δ3, and that DVMAT-Y600A acts as either a gain-of-function "neomorphic" allele or a dominant negative in some circuits.

Discussion

The trafficking of vesicular neurotransmitters has been extensively studied in cultured cell lines and primary neu-
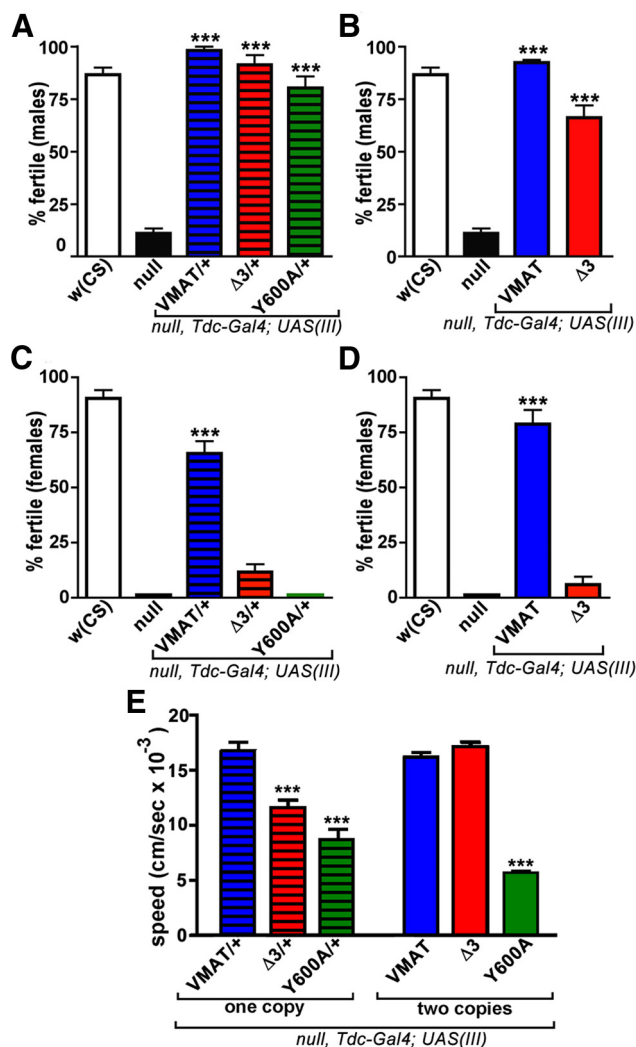
Figure 9. Rescue with *Tdc2-Gal4* reveals behavioral defects for DVMAT-Y600A. **A**, **B**, Male fertility. The infertility defect of the *dVMAT[P1]* null can be rescued to near w(CS) control levels using one copy of *UAS-DVMAT-wt* and one copy of the *Tdc2-Gal4* driver (**A**) or two copies of both the *UAS-DVMAT-wt* and *Tdc2-Gal4* drivers (**B**; one-way ANOVA, $p < 0.0001$; Bonferroni post-test, ***$p < 0.001$ compared with *dVMAT[P1]* nulls; $n \geq 49$ matings per genotype for **A–D**). Either one (**A**) or two (**B**) copies of *Tdc2-Gal4* plus *UAS-DVMAT-Δ3* rescued male fertility. **A**, One copy of *Tdc2-Gal4* plus *UAS DVMAT-Y600A* rescued male fertility. **C**, **D**, Female fertility. Either one (**C**) or two (**D**) copies of *UAS-DVMAT-wt* coupled with one or two copies of *Tdc2-Gal4*, respectively, rescued female fertility (Bonferroni post-test, ***$p < 0.001$ compared with *dV-MAT[P1]* nulls). Neither one (**C**) nor two (**D**) copies of *UAS-DVMAT-Δ3* coupled with one or two copies of *Tdc2-Gal4*, respectively, rescued female fertility. One copy of *Tdc2-Gal4* plus one copy of *UAS-DVMAT-Y600A* also failed to rescue female fertility. (Flies expressing two copies of *Tdc2-Gal4* plus two copies of *UAS-DVMAT-Y600A* were not viable as adults, thus preventing fertility assays in **B–D**.) **E**, Larval locomotion. Third-instar *dVMAT[P1]* null larvae expressing one or two copies (as indicated) of *UAS-DVMAT-wt*, *UAS-DVMAT-Δ3*, or *UAS-DVMAT-Y600A* plus one or two copies, respectively, of the *Tdc2-Gal4* driver were assayed for locomotion. Compared with *DVMAT-wt*, *DVMAT-Δ3* showed partial rescue of the *dVMAT[P1]* null locomotion deficit using one copy of the UAS transgene plus driver, and full rescue using two copies of transgene plus driver. *DVMAT-Y600A* showed partial rescue with one copy that did not improve using two copies. (Two-way ANOVA, $n = 9–12$ animals per genotype, $p < 0.0001$ for genotype and interaction; Bonferroni post-test, one-copy mutant vs wt or two-copy mutant vs wild-type, ***$p < 0.001$).

ronal cultures *in vitro* (Tan et al., 1998; Varoqui and Erickson, 1998; Krantz et al., 2000; Waites et al., 2001; Barbosa et al., 2002; Ferreira et al., 2005; Voglmaier et al., 2006; Colgan et al., 2007; Fleckenstein et al., 2007; Yao and Hersh, 2007; Asensio et al., 2010). However, it has remained unclear how changes in the
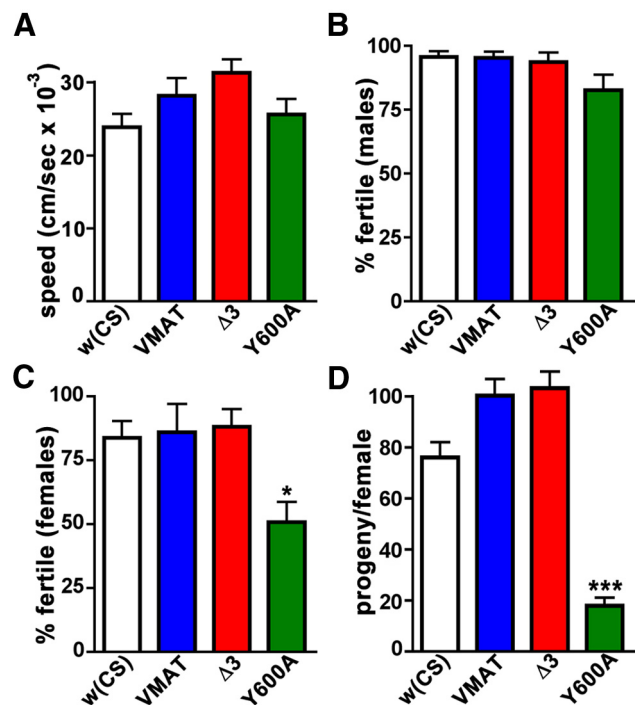
Figure 10. **A**, **B**, Dominant effects of DVMAT-Y600A. Larval locomotion (**A**, $n = 7$ trials/genotype) and male fertility (**B**, $n \geq 44$ matings/genotype) are minimally compromised by the expression of two copies of *UAS-DVMAT-Y600A* (or other *DVMAT* transgenes) using two copies of the *Tdc2-Gal4* driver in a wild-type *dVMAT* background. **C**, **D**, In contrast, overexpression of the *UAS-DVMAT-Y600A* (third chromosome) transgene under these conditions results in reduced female fertility (**C**, one-way ANOVA, $p < 0.03$; Bonferroni post-test, *$p < 0.05$ comparing *UAS-DVMAT-Y600A* to either *UAS-DVMAT-wt* or *UAS-DVMAT-Δ3*, $n \geq 44$ matings/genotype) and a decrease in the number of progeny (**D**, one-way ANOVA $p < 0.0001$; Bonferroni post-test, ***$p < 0.001$ comparing *UAS-DVMAT-Y600A* to *UAS-DVMAT-wt* or *UAS-DVMAT-Δ3*, $n \geq 26$ matings/genotype), suggesting a dominant effect for *UAS-DVMAT-Y600A* distinct from that for either *UAS-DVMAT-wt* or *UAS-DVMAT-Δ3*.

trafficking of VMATs (or any other vesicular transporter) might influence their function in the nervous system as a whole. Using mutations in DVMAT, we show here that *in vivo* alterations of transporter trafficking have dramatic effects on a subset of behaviors. We speculate that the specific behavioral changes we observe with DVMAT-Δ3 and DVMAT-Y600A mutants result from alterations in their relative distribution of DVMAT to SVs versus to LDCVs. By extension, these results suggest that the balance between amine release by SVs and LDCVs is critical for the function of some aminergic circuits. Interestingly, an increase in stimulated secretion via LDCVs has been associated with case studies of autism (Castermans et al., 2010).

Vesicular transporters sort to SVs or LDCVs through two distinct pathways (Liu et al., 1999). Targeting to SVs requires exit from the trans-Golgi network (TGN) on constitutive secretory vesicles, followed by endocytosis at the plasma membrane (Hannah et al., 1999; Fei et al., 2008). *De novo* targeting of the transporters to LDCVs requires a distinct set of trafficking events, including sorting into the regulated secretory pathway at the TGN (Gu et al., 2001; Morvan and Tooze, 2008; Park et al., 2011). Some of the signals for these pathways have been identified using *in vitro* cellular models (for review, see Fei et al., 2008), but others remain unclear. In addition, the possible interplay between sorting to SVs versus to LDCVs in neurons has remained speculative (Fei et al., 2008), despite accumulating evidence that this occurs in neuroendocrine cell lines (Norcott et al., 1996; Blagoveshchenskaya et al., 1999; Krantz et al., 2000).

In a previous report, deletion of the terminal 23 aa of DVMAT in DVMAT-Δ3 resulted in reduced localization to SVs (Grygoruk et al., 2010). Our finding that DVMAT-Δ3 slows endocytosis at the nerve terminal is consistent with the proposed requirement of endocytosis for *de novo* sorting and recycling to SVs (Fei et al., 2008). Conversely, DVMAT-Δ3 retained the ability to sort to LDCVs, and, when expressed in aminergic cells, localized to LDCVs to a greater degree than DVMAT-wt. It remains possible that DVMAT-Δ3 and DVMAT-wt could sort to distinct subtypes of LDCVs (e.g., to those less or more competent for exocytotic release; Zhang et al., 2011; Hugo et al., 2013). If so, this too, might affect the downstream behavioral phenotype of flies expressing each variant.

The breakpoint of Δ3 occurs between the acidic (DE) and dileucine (LI) signals, such that the DE motif (amino acids 584 and 585), which has been shown to be essential for the localization of mammalian VMAT2 to LDCVs (Waites et al., 2001; Li et al., 2005), is retained, while the downstream LI motif is absent (Fig. 1*A*). Although the DE site in DVMAT might be expected to work in concert with a downstream LI as part of the extended dileucine motif (Bonifacino and Traub, 2003; Asensio et al., 2010), the localization of DVMAT-Δ3 to LDCVs in the absence of the LI signal suggests that the acidic motif alone may allow sorting of DVMAT to LDCVs, at least in *Drosophila*. Alternatively, other sequences may compensate for disruption of the extended dileucine motif. The lumenal domain of mammalian VMAT2 may help to promote trafficking to LDCVs in PC12 cells (Yao and Hersh, 2007). The LDCV protein phogrin contains at least three distinct signals that contribute to sorting to LDCVs, including cytosolic tyrosine (Wasmeier et al., 2005) and dileucine motifs (Torii et al., 2005), as well as a lumenal signal (Wasmeier et al., 2002). The relative importance of each cytosolic signal is dependent on the presence or absence of the other motif (Torii et al., 2005; Wasmeier et al., 2005).

Interestingly, the observed shift to LDCVs of DVMAT mutants lacking active signaling motifs suggests that LDCVs could represent the "default" localization for DVMAT. We emphasize that this would not contradict the idea that the default pathway for sorting VMATs during TGN exit is likely to be the constitutive secretory pathway (Li et al., 2005). Multiple trafficking events beyond those at the TGN and plasma membrane may contribute to the baseline localization of DVMAT. These might include LDCV recycling pathways or recently characterized post-endocytic compartments that regulate SV trafficking at the synapse, both of which remain poorly understood (Uytterhoeven et al., 2011; Trueta et al., 2012). Our data on the localization of DVMAT represent the sum of all of these events rather than individual sorting steps in either the secretory or endocytic pathways.

In this study, we also illustrate a novel involvement for cellular context in deciphering DVMAT trafficking motifs. Unexpectedly, we observe significant differences in DVMAT trafficking between aminergic and non-aminergic cells. DVMAT-Y600A showed a defect in endocytosis in aminergic type II terminals, but not in glutamatergic type Ib terminals. Thus, the endocytic mechanisms in aminergic versus nonaminergic cells may differ for DVMAT, as suggested by studies of mammalian VMAT2 in hippocampal and midbrain dopaminergic neuronal cultures (Onoa et al., 2010). Further analysis of DVMAT may be useful to define the mechanistic differences between endocytosis in aminergic versus non-aminergic neurons, as well as potential differences in other trafficking steps. Although DVMAT-Y600A, like DVMAT-Δ3, showed an increased localization to LDCVs, the SV sorting defect for Y600A appeared to be more severe in aminergic neu-

rons. Furthermore, when expressed primarily in nonaminergic cells using *elav-Gal4*, DVMAT-Δ3 localized in part to an ectopic peak in sucrose gradients; DVMAT-Y600A did not show a detectable peak at this position. We speculate that variations in the fractionation of DVMAT mutants may result from functional differences between aminergic and non-aminergic trafficking pathways (e.g., sorting and recycling to larger numbers of LDCVs in aminergic neurons; Straley and Green, 2000; Bäck et al., 2010).

The precise mechanisms by which Y600A and Δ3 control the localization of DVMAT to SVs versus LDCVs, and how these processes diverge across different types of neurons, will be investigated in future experiments, in part via genetic interactions with other mutations that affect known components of the trafficking machinery (González-Gaitán and Jäckle, 1997; Dickman et al., 2005; Asensio et al., 2010). Here, we have first taken advantage of the observed cellular phenotypes of DVMAT-Δ3 and DVMAT-Y600A to determine whether altering the distribution of DVMAT between SVs and LDCVs would have a detectable effect on behavior.

When expressed at moderate levels using the broadly expressed driver *da-Gal4*, DVMAT-Δ3 rescues larval locomotion, survival, and male fertility similarly to DVMAT-wt, but fails to rescue female fertility and egg laying. Similar effects were observed when DVMAT-Δ3 was expressed more specifically in octopaminergic neurons. Since the *UAS-DVMAT-Δ3* transgene clearly rescued some but not other aspects of the *dVMAT^P1* null phenotype, it behaves as a partial loss-of-function, or hypomorphic, allele (Muller, 1932; Wilkie, 1994). This may result from a decreased ability to sort to SVs. This, in turn would suggest that storage in and release from SVs is critical for the function of some aminergic circuits in the fly. However, since DVMAT-Δ3 also shows an increased localization to LDCVs in aminergic cells, we speculate that both decreased amine storage in SVs and increased storage in LDCVs may contribute to the phenotype of DVMAT-Δ3, and that the behavioral phenotype we observe is due to disruption of the usual balance of release from SVs and LDCVs.

The behavioral defects of DVMAT-Y600A are distinct from those observed for DVMAT-Δ3, and we propose that they reflect the observed differences in their trafficking. When expressed broadly using *da-Gal4*, DVMAT-Y600A behaves similarly to DVMAT-wt and appears to rescue most behaviors, including female fertility. However, when expressed in octopaminergic neurons using *Tdc2-Gal4*, DVMAT-Y600A behaves as a more severe allele than DVMAT-Δ3, and disrupts both female fertility and larval locomotion. In addition, when expressed at high levels, DVMAT-Y600A shows a more severe dominant effect than either DVMAT-wt or DVMAT-Δ3. We propose that these dominant effects and the observed differences in the behavioral phenotype of DVMAT-Δ3 and DVMAT-Y600A result from a more severely imbalanced distribution between LDCVs and SVs that we observe when the mutants are expressed in aminergic neurons.

We are intrigued by the observation that some behaviors appear to be particularly sensitive to changes in DVMAT trafficking. It is possible that the circuits mediating these behaviors require a relatively high degree of spatial or temporal precision that is only possible via SV release at the synapse. Egg laying requires both rhythmic contraction of the musculoepithelial net surrounding the ovary as well relaxation of the oviduct (Lee et al., 2003, 2009; Monastirioti, 2003; Middleton et al., 2006), and coordination of these activities may be particularly sensitive to shifting DVMAT from SVs to LDCVs.

Further study of these and other circuits that are affected by DVMAT trafficking may help to determine the mechanisms by

which alterations in amine release modulate behavior. Such studies may also be useful to understand the long-term behavioral responses to psychostimulants and antidepressants, both of which are thought to be critically dependent on the site and manner of amine release (Kalivas and Duffy, 1993a,b; Blier et al., 1998; Adell et al., 2002; Vezina, 2004; Li et al., 2005; Sarter et al., 2007; Colgan et al., 2009; Richardson-Jones et al., 2010).

References

Adell A, Celada P, Abellán MT, Artigas F (2002) Origin and functional role of the extracellular serotonin in the midbrain raphe nuclei. Brain Res Brain Res Rev 39:154–180. CrossRef Medline

Akbar MA, Ray S, Krämer H (2009) The SM protein Car/Vps33A regulates SNARE-mediated trafficking to lysosomes and lysosome-related organelles. Mol Biol Cell 20:1705–1714. CrossRef Medline

Asensio CS, Sirkis DW, Edwards RH (2010) RNAi screen identifies a role for adaptor protein AP-3 in sorting to the regulated secretory pathway. J Cell Biol 191:1173–1187. CrossRef Medline

Atwood HL, Govind CK, Wu CF (1993) Differential ultrastructure of synaptic terminals on ventral longitudinal abdominal muscles in Drosophila larvae. J Neurobiol 24:1008–1024. CrossRef Medline

Bäck N, Rajagopal C, Mains RE, Eipper BA (2010) Secretory granule membrane protein recycles through multivesicular bodies. Traffic 11:972–986. CrossRef Medline

Barbosa J Jr, Ferreira LT, Martins-Silva C, Santos MS, Torres GE, Caron MG, Gomez MV, Ferguson SS, Prado MA, Prado VF (2002) Trafficking of the vesicular acetylcholine transporter in SN56 cells: a dynamin-sensitive step and interaction with the AP-2 adaptor complex. J Neurochem 82:1221–1228. CrossRef Medline

Benzer S (1967) Behavioral mutants of Drosophila isolated by countercurrent distribution. Proc Natl Acd Sci USA 58:1112–1119.

Birman S, Morgan B, Anzivino M, Hirsh J (1994) A novel and major isoform of tyrosine hydroxylase in Drosophila is generated by alternative RNA processing. J Biol Chem 269:26559–26567. Medline

Blagoveshchenskaya AD, Hewitt EW, Cutler DF (1999) A complex web of signal-dependent trafficking underlies the triorganellar distribution of P-selectin in neuroendocrine PC12 cells. J Cell Biol 145:1419–1433. CrossRef Medline

Blakely RD, Edwards RH (2012) Vesicular and plasma membrane transporters for neurotransmitters. Cold Spring Harb Perspect Biol 4:a005595. CrossRef Medline

Blier P, Piñeyro G, el Mansari M, Bergeron R, de Montigny C (1998) Role of somatodendritic 5-HT autoreceptors in modulating 5-HT neurotransmission. Ann N Y Acad Sci 861:204–216. CrossRef Medline

Bonifacino JS, Traub LM (2003) Signals for sorting of transmembrane proteins to endosomes and lysosomes. Annu Rev Biochem 72:395–447. CrossRef Medline

Brand AH, Perrimon N (1993) Targeted gene expression as a means of altering cell fates and generating dominant phenotypes. Development 118:401–415. Medline

Bruns D, Jahn R (1995) Real-time measurement of transmitter release from single synaptic vesicles. Nature 377:62–65. CrossRef Medline

Bruns D, Riedel D, Klingauf J, Jahn R (2000) Quantal release of serotonin. Neuron 28:205–220. CrossRef Medline

Budnik V, Gorczyca M, Prokop A (2006) Selected methods for the anatomical study of Drosophila embryonic and larval neuromuscular junctions. Int Rev Neurobiol 75:323–365. CrossRef Medline

Castermans D, Volders K, Crepel A, Backx L, De Vos R, Freson K, Meulemans S, Vermeesch JR, Schrander-Stumpel CT, De Rijk P, Del-Favero J, Van Geet C, Van De Ven WJ, Steyaert JG, Devriendt K, Creemers JW (2010) SCAMP5, NBEA and AMISYN: three candidate genes for autism involved in secretion of large dense-core vesicles. Hum Mol Genet 19:1368–1378. CrossRef Medline

Caudy M, Vässin H, Brand M, Tuma R, Jan LY, Jan YN (1988) daughterless, a Drosophila gene essential for both neurogenesis and sex determination, has sequence similarities to myc and the achaete-scute complex. Cell 55:1061–1067. CrossRef Medline

Chang HY, Grygoruk A, Brooks ES, Ackerson LC, Maidment NT, Bainton RJ, Krantz DE (2006) Over-expression of the Drosophila vesicular monoamine transporter increases motor activity and courtship but decreases the behavioral response to cocaine. Mol Psychiatry 11:99–113. CrossRef Medline

Chen A, Ng F, Lebestky T, Grygoruk A, Djapri C, Lawal HO, Zaveri HA, Mehanzel F, Najibi R, Seidman G, Murphy NP, Kelly RL, Ackerson LC, Maidment NT, Jackson FR, Krantz DE (2013) Dispensable, redundant, complementary, and cooperative roles of dopamine, octopamine, and serotonin in Drosophila melanogaster. Genetics 193:159–176. CrossRef Medline

Cole SH, Carney GE, McClung CA, Willard SS, Taylor BJ, Hirsh J (2005) Two functional but noncomplementing Drosophila tyrosine decarboxylase genes: distinct roles for neural tyramine and octopamine in female fertility. J Biol Chem 280:14948–14955. CrossRef Medline

Colgan LA, Putzier I, Levitan ES (2009) Activity-dependent vesicular monoamine transporter-mediated depletion of the nucleus supports somatic release by serotonin neurons. J Neurosci 29:15878–15887. CrossRef Medline

Colgan L, Liu H, Huang SY, Liu YJ (2007) Dileucine motif is sufficient for internalization and synaptic vesicle targeting of vesicular acetylcholine transporter. Traffic 8:512–522. CrossRef Medline

Collins CA, DiAntonio A (2007) Synaptic development: insights from Drosophila. Curr Opin Neurobiol 17:35–42. CrossRef Medline

Connolly JB, Tully T (1998) Behaviour, learning and memory. In: Drosophila, a practical approach, Ed 2 (Roberts DB, ed), pp 265–317. Oxford, UK: IRL.

Davis GW (2006) Homeostatic control of neural activity: from phenomenology to molecular design. Annu Rev Neurosci 29:307–323. CrossRef Medline

De-Miguel FF, Trueta C (2005) Synaptic and extrasynaptic secretion of serotonin. Cell Mol Neurobiol 25:297–312. CrossRef Medline

Dickman DK, Horne JA, Meinertzhagen IA, Schwarz TL (2005) A slowed classical pathway rather than kiss-and-run mediates endocytosis at synapses lacking synaptojanin and endophilin. Cell 123:521–533. CrossRef Medline

Dreosti E, Lagnado L (2011) Optical reporters of synaptic activity in neural circuits. Exp Physiol 96:4–12. CrossRef Medline

Eiden LE, Weihe E (2011) VMAT2: a dynamic regulator of brain monoaminergic neuronal function interacting with drugs of abuse. Ann N Y Acad Sci 1216:86–98. CrossRef Medline

Emery G, Hutterer A, Berdnik D, Mayer B, Wirtz-Peitz F, Gaitan MG, Knoblich JA (2005) Asymmetric Rab 11 endosomes regulate delta recycling and specify cell fate in the Drosophila nervous system. Cell 122:763–773. CrossRef Medline

Entchev EV, Schwabedissen A, González-Gaitán M (2000) Gradient formation of the TGF-beta homolog Dpp. Cell 103:981–991. CrossRef Medline

Fei H, Grygoruk A, Brooks ES, Chen A, Krantz DE (2008) Trafficking of vesicular neurotransmitter transporters. Traffic 9:1425–1436. CrossRef Medline

Feng Y, Ueda A, Wu CF (2004) A modified minimal hemolymph-like solution, HL3.1, for physiological recordings at the neuromuscular junctions of normal and mutant Drosophila larvae. J Neurogenet 18:377–402. CrossRef Medline

Ferreira LT, Santos MS, Kolmakova NG, Koenen J, Barbosa J Jr, Gomez MV, Guatimosim C, Zhang X, Parsons SM, Prado VF, Prado MA (2005) Structural requirements for steady-state localization of the vesicular acetylcholine transporter. J Neurochem 94:957–969. CrossRef Medline

Fleckenstein AE, Volz TJ, Riddle EL, Gibb JW, Hanson GR (2007) New insights into the mechanism of action of amphetamines. Annu Rev Pharmacol Toxicol 47:681–698. CrossRef Medline

Fon EA, Pothos EN, Sun BC, Killeen N, Sulzer D, Edwards RH (1997) Vesicular transport regulates monoamine storage and release but is not essential for amphetamine action. Neuron 19:1271–1283. CrossRef Medline

González-Gaitán M, Jäckle H (1997) Role of Drosophila alpha-adaptin in presynaptic vesicle recycling. Cell 88:767–776. CrossRef Medline

Greer CL, Grygoruk A, Patton DE, Ley B, Romero-Calderon R, Chang HY, Houshyar R, Bainton RJ, Diantonio A, Krantz DE (2005) A splice variant of the Drosophila vesicular monoamine transporter contains a conserved trafficking domain and functions in the storage of dopamine, serotonin and octopamine. J Neurobiol 64:239–258. CrossRef Medline

Grygoruk A, Fei H, Daniels RW, Miller BR, Diantonio A, Krantz DE (2010) A tyrosine-based motif localizes a Drosophila vesicular transporter to synaptic vesicles in vivo. J Biol Chem 285:6867–6878. CrossRef Medline

Gu F, Crump CM, Thomas G (2001) Trans-Golgi network sorting. Cell Mol Life Sci 58:1067–1084. CrossRef Medline

Hannah MJ, Schmidt AA, Huttner WB (1999) Synaptic vesicle biogenesis. Annu Rev Cell Dev Biol 15:733–798. CrossRef Medline

Hirsh J, Davidson N (1981) Isolation and characterization of the dopa decarboxylase gene of Drosophila melanogaster. Mol Cell Biol 1:475–485. Medline

Hugo S, Dembla E, Halimani M, Matti U, Rettig J, Becherer U (2013) Deciphering dead-end docking of large dense core vesicles in bovine chromaffin cells. J Neurosci 33:17123–17137. CrossRef Medline

Kalivas PW, Duffy P (1993a) Time course of extracellular dopamine and behavioral sensitization to cocaine. I. Dopamine axon terminals. J Neurosci 13:266–275. Medline

Kalivas PW, Duffy P (1993b) Time course of extracellular dopamine and behavioral sensitization to cocaine. II. Dopamine perikarya. J Neurosci 13:276–284. Medline

Kelly RB (1993) Storage and release of neurotransmitters. Cell 10 [Suppl]:43–53.

Krantz DE, Waites C, Oorschot V, Liu Y, Wilson RI, Tan PK, Klumperman J, Edwards RH (2000) A phosphorylation site regulates sorting of the vesicular acetylcholine transporter to dense core vesicles. J Cell Biol 149:379–396. CrossRef Medline

Kuffler DP, Nicholls J, Drapeau P (1987) Transmitter localization and vesicle turnover at a serotoninergic synapse between identified leech neurons in culture. J Comp Neurol 256:516–526. CrossRef Medline

Lawal HO, Krantz DE (2013) SLC18: vesicular neurotransmitter transporters for monoamines and acetylcholine. Mol Aspects Med 34:360–372. CrossRef Medline

Lee HG, Seong CS, Kim YC, Davis RL, Han KA (2003) Octopamine receptor OAMB is required for ovulation in Drosophila melanogaster. Dev Biol 264:179–190. CrossRef Medline

Lee HG, Rohila S, Han KA (2009) The octopamine receptor OAMB mediates ovulation via Ca2+/calmodulin-dependent protein kinase II in the Drosophila oviduct epithelium. PLoS One 4:e4716. CrossRef Medline

Levitan ES (2008) Signaling for vesicle mobilization and synaptic plasticity. Mol Neurobiol 37:39–43. CrossRef Medline

Li H, Waites CL, Staal RG, Dobryy Y, Park J, Sulzer DL, Edwards RH (2005) Sorting of vesicular monoamine transporter 2 to the regulated secretory pathway confers the somatodendritic exocytosis of monoamines. Neuron 48:619–633. CrossRef Medline

Liu Y, Schweitzer ES, Nirenberg MJ, Pickel VM, Evans CJ, Edwards RH (1994) Preferential localization of a vesicular monoamine transporter to dense core vesicles in PC12 cells. J Cell Biol 127:1419–1433. CrossRef Medline

Liu Y, Krantz DE, Waites C, Edwards RH (1999) Membrane trafficking of neurotransmitter transporters in the regulation of synaptic transmission. Trends Cell Biol 9:356–363. CrossRef Medline

Middleton CA, Nongthomba U, Parry K, Sweeney ST, Sparrow JC, Elliott CJ (2006) Neuromuscular organization and aminergic modulation of contractions in the Drosophila ovary. BMC Biol 4:17. CrossRef Medline

Miesenböck G, De Angelis DA, Rothman JE (1998) Visualizing secretion and synaptic transmission with pH-sensitive green fluorescent proteins. Nature 394:192–195. CrossRef Medline

Monastirioti M (1999) Biogenic amine systems in the fruit fly Drosophila melanogaster. Microsc Res Tech 45:106–121. CrossRef Medline

Monastirioti M (2003) Distinct octopamine cell population residing in the CNS abdominal ganglion controls ovulation in Drosophila melanogaster. Dev Biol 264:38–49. CrossRef Medline

Monastirioti M, Gorczyca M, Rapus J, Eckert M, White K, Budnik V (1995) Octopamine immunoreactivity in the fruit fly Drosophila melanogaster. J Comp Neurol 356:275–287. CrossRef Medline

Monastirioti M, Linn CE Jr, White K (1996) Characterization of Drosophila tyramine beta-hydroxylase gene and isolation of mutant flies lacking octopamine. J Neurosci 16:3900–3911. Medline

Morvan J, Tooze SA (2008) Discovery and progress in our understanding of the regulated secretory pathway in neuroendocrine cells. Histochem Cell Biol 129:243–252. CrossRef Medline

Muller HJ (1932) Further studies on the nature and causes of gene mutations. In: Proceedings of the 6th International Congress of Genetics (Jones DF, ed), pp 213–255. Bethesda, MD: Genetics Society of America.

Neckameyer WS, White K (1993) Drosophila tyrosine hydroxylase is encoded by the pale locus. J Neurogenet 8:189–199. CrossRef Medline

Nirenberg MJ, Chan J, Liu Y, Edwards RH, Pickel VM (1997) Vesicular monoamine transporter-2: immunogold localization in striatal axons and terminals. Synapse 26:194–198. CrossRef Medline

Norcott JP, Solari R, Cutler DF (1996) Targeting of P-selectin to two regulated secretory organelles in PC12 cells. J Cell Biol 134:1229–1240. CrossRef Medline

Oh SW, Kingsley T, Shin HH, Zheng Z, Chen HW, Chen X, Wang H, Ruan P, Moody M, Hou SX (2003) A P-element insertion screen identified mutations in 455 novel essential genes in Drosophila. Genetics 163:195–201. Medline

Onoa B, Li H, Gagnon-Bartsch JA, Elias LA, Edwards RH (2010) Vesicular monoamine and glutamate transporters select distinct synaptic vesicle recycling pathways. J Neurosci 30:7917–7927. CrossRef Medline

Park JJ, Gondré-Lewis MC, Eiden LE, Loh YP (2011) A distinct trans-Golgi network subcompartment for sorting of synaptic and granule proteins in neurons and neuroendocrine cells. J Cell Sci 124:735–744. CrossRef Medline

Pizzo AB, Karam CS, Zhang Y, Yano H, Freyberg RJ, Karam DS, Freyberg Z, Yamamoto A, McCabe BD, Javitch JA (2013) The membrane-raft protein Flotillin-1 is essential in dopamine neurons for amphetamine-induced behavior in Drosophila. Mol Psychiatry 18:824–833. CrossRef Medline

Pulipparacharuvil S, Akbar MA, Ray S, Sevrioukov EA, Haberman AS, Rohrer J, Krämer H (2005) Drosophila Vps16A is required for trafficking to lysosomes and biogenesis of pigment granules. J Cell Sci 118:3663–3673. CrossRef Medline

Rao S, Lang C, Levitan ES, Deitcher DL (2001) Visualization of neuropeptide expression, transport, and exocytosis in Drosophila melanogaster. J Neurobiol 49:159–172. CrossRef Medline

Richardson-Jones JW, Craige CP, Guiard BP, Stephen A, Metzger KL, Kung HF, Gardier AM, Dranovsky A, David DJ, Beck SG, Hen R, Leonardo ED (2010) 5-HT1A autoreceptor levels determine vulnerability to stress and response to antidepressants. Neuron 65:40–52. CrossRef Medline

Robinow S, White K (1988) The locus elav of Drosophila melanogaster is expressed in neurons at all developmental stages. Dev Biol 126:294–303. CrossRef Medline

Roeder T (2005) Tyramine and octopamine: ruling behavior and metabolism. Annu Rev Entomol 50:447–477. CrossRef Medline

Romero-Calderón R, Uhlenbrock G, Borycz J, Simon AF, Grygoruk A, Yee SK, Shyer A, Ackerson LC, Maidment NT, Meinertzhagen IA, Hovemann BT, Krantz DE (2008) A glial variant of the vesicular monoamine transporter is required to store histamine in the Drosophila visual system. PLoS Genet 4:e1000245. CrossRef Medline

Sankaranarayanan S, D De Angelis D, Rothman JE, Ryan TA (2000) The use of pHluorins for optical measurements of presynaptic activity. Biophys J 79:2199–2208. CrossRef Medline

Sarter M, Bruno JP, Parikh V (2007) Abnormal neurotransmitter release underlying behavioral and cognitive disorders: toward concepts of dynamic and function-specific dysregulation. Neuropsychopharmacology 32:1452–1461. CrossRef Medline

Simon AF, Liang DT, Krantz DE (2006) Differential decline in behavioral performance of Drosophila melanogaster with age. Mech Ageing Dev 127:647–651. CrossRef Medline

Simon AF, Daniels R, Romero-Calderón R, Grygoruk A, Chang HY, Najibi R, Shamouelian D, Salazar E, Solomon M, Ackerson LC, Maidment NT, Diantonio A, Krantz DE (2009) Drosophila vesicular monoamine transporter mutants can adapt to reduced or eliminated vesicular stores of dopamine and serotonin. Genetics 181:525–541. CrossRef Medline

St Johnston D (2013) Using mutants, knockdowns, and transgenesis to investigate gene function in Drosophila. Wiley Interdiscip Rev Dev Biol 2:587–613. CrossRef Medline

Straley KS, Green SA (2000) Rapid transport of internalized P-selectin to late endosomes and the TGN: roles in regulating cell surface expression and recycling to secretory granules. J Cell Biol 151:107–116. CrossRef Medline

Südhof TC, Rizo J (2011) Synaptic vesicle exocytosis. Cold Spring Harb Perspect Biol 3:a005637. CrossRef Medline

Swierczek NA, Giles AC, Rankin CH, Kerr RA (2011) High-throughput behavioral analysis in C. elegans. Nat Methods 8:592–598. CrossRef Medline

Tan PK, Waites C, Liu Y, Krantz DE, Edwards RH (1998) A leucine-based motif mediates the endocytosis of vesicular monoamine and acetylcholine transporters. J Biol Chem 28:17351–17360.

Thureson-Klein A (1983) Exocytosis from large and small dense cored ves-

icles in noradrenergic nerve terminals. Neuroscience 10:245–259. CrossRef Medline

Torii S, Saito N, Kawano A, Zhao S, Izumi T, Takeuchi T (2005) Cytoplasmic transport signal is involved in phogrin targeting and localization to secretory granules. Traffic 6:1213–1224. CrossRef Medline

Trueta C, Kuffler DP, De-Miguel FF (2012) Cycling of dense core vesicles involved in somatic exocytosis of serotonin by leech neurons. Front Physiol 3:175. CrossRef Medline

Uytterhoeven V, Kuenen S, Kasprowicz J, Miskiewicz K, Verstreken P (2011) Loss of skywalker reveals synaptic endosomes as sorting stations for synaptic vesicle proteins. Cell 145:117–132. CrossRef Medline

van de Goor J, Ramaswami M, Kelly R (1995) Redistribution of synaptic vesicles and their proteins in temperature-sensitive shibire(ts1) mutant Drosophila. Proc Natl Acad Sci U S A 92:5739–5743. CrossRef Medline

Varoqui H, Erickson JD (1998) The cytoplasmic tail of the vesicular acetylcholine transporter contains a synaptic vesicle targeting signal. J Biol Chem 273:9094–9098. CrossRef Medline

Vezina P (2004) Sensitization of midbrain dopamine neuron reactivity and the self-administration of psychomotor stimulant drugs. Neurosci Biobehav Rev 27:827–839. CrossRef Medline

Voglmaier SM, Kam K, Yang H, Fortin DL, Hua Z, Nicoll RA, Edwards RH (2006) Distinct endocytic pathways control the rate and extent of synaptic vesicle protein recycling. Neuron 51:71–84. CrossRef Medline

Vömel M, Wegener C (2008) Neuroarchitecture of aminergic systems in the larval ventral ganglion of Drosophila melanogaster. PLoS One 3:e1848. CrossRef Medline

Waites CL, Mehta A, Tan PK, Thomas G, Edwards RH, Krantz DE (2001) An acidic motif retains vesicular monoamine transporter 2 on large dense core vesicles. J Cell Biol 152:1159–1168. CrossRef Medline

Wasmeier C, Bright NA, Hutton JC (2002) The lumenal domain of the integral membrane protein phogrin mediates targeting to secretory granules. Traffic 3:654–665. CrossRef Medline

Wasmeier C, Burgos PV, Trudeau T, Davidson HW, Hutton JC (2005) An extended tyrosine-targeting motif for endocytosis and recycling of the dense-core vesicle membrane protein phogrin. Traffic 6:474–487. CrossRef Medline

Wilkie AO (1994) The molecular basis of genetic dominance. J Med Genet 31:89–98. CrossRef Medline

Wong MY, Zhou C, Shakiryanova D, Lloyd TE, Deitcher DL, Levitan ES (2012) Neuropeptide delivery to synapses by long-range vesicle circulation and sporadic capture. Cell 148:1029–1038. CrossRef Medline

Wright TR (1996) The Wilhelmine E. Key 1992 Invitational lecture. Phenotypic analysis of the Dopa decarboxylase gene cluster mutants in Drosophila melanogaster. J Hered 87:175–190. CrossRef Medline

Wucherpfennig T, Wilsch-Bräuninger M, González-Gaitán M (2003) Role of Drosophila Rab5 during endosomal trafficking at the synapse and evoked neurotransmitter release. J Cell Biol 161:609–624. CrossRef Medline

Yao J, Hersh LB (2007) The vesicular monoamine transporter 2 contains trafficking signals in both its N-glycosylation and C-terminal domains. J Neurochem 100:1387–1396. CrossRef Medline

Yao J, Erickson JD, Hersh LB (2004) Protein kinase A affects trafficking of the vesicular monoamine transporters in PC12 cells. Traffic 5:1006–1016. CrossRef Medline

Zhang YQ, Rodesch CK, Broadie K (2002) Living synaptic vesicle marker: synaptotagmin-GFP. Genesis 34:142–145. CrossRef Medline

Zhang Z, Wu Y, Wang Z, Dunning FM, Rehfuss J, Ramanan D, Chapman ER, Jackson MB (2011) Release mode of large and small dense-core vesicles specified by different synaptotagmin isoforms in PC12 cells. Mol Biol Cell 22:2324–2336. CrossRef Medline

Zinsmaier KE, Hofbauer A, Heimbeck G, Pflugfelder GO, Buchner S, Buchner E (1990) A cysteine-string protein is expressed in retina and brain of Drosophila. J Neurogenet 7:15–29. CrossRef Medline